Mitochondrial accumulation induced axon dysfunction promotes paranode instability and demyelination in hypoxic-ischemic forms of demyelination

Mei Cui (cuimei@fudan.edu.cn)
University of Rochester
Yiwei Feng
Huashan Hospital
Min Guo
Huashan Hospital
Hongchen Zhao
Huashan Hospital
Sida Han
Huashan Hospital
Yanxing Zhao
Shanghai Tenth People's Hospital
Qiang Dong
Huashan Hospital, Fudan University https://orcid.org/0000-0001-6630-112X

Article

Keywords: demyelination, paranode stability, mitochondria, syntaphilin, hypoperfusion

Posted Date: November 14th, 2020

DOI: https://doi.org/10.21203/rs.3.rs-102169/v1

Abstract

Hypoxic-ischemic forms of demyelination, caused by chronic or acute reduction of blood flow in subcortical white matter, is increasingly considered as an important contributor to cognitive decline. However, it remains unclear how hypoxia/ischemia leads to demyelination pathology and no effective drugs clinically. In this study, we aimed to investigate the relationship between axon injuries and demyelination as well as the mechanism in the development of hypoxic-ischemic forms of demyelination. Bilateral common carotid artery stenosis (BCAS) mouse model of whole-brain hypoperfusion was used to observe the pathological changes of hypoperfusion-induced demyelination in vivo, and low glucose-low oxygen (LGLO) treatment in cerebellum slice cultures was used to uncover molecular machinery in vitro. We found that mitochondria were excessively accumulated among axons after BCAS/LGLO, which impaired the retrograde transport of mitochondria for mitophagy and anterograde transport for metabolic supply. This axonal insult occurred prior to demyelination and promoted the progression of demyelination through impairing the paranode stability by mitochondrial ROS. Syntaphilin (SNPH), an axonal specific arching protein of mitochondria, was elevated after hypoperfusion and was responsible for the accumulation of mitochondria. Knockdown of SNPH promoted retrograde transport of mitochondria to alleviate ROS load among axons and enhanced anterograde transport of mito-chondria for synapse signalling, mitigated demyelination and retrieved cognitive function. Our results uncovered a distinctive pathological characteristic of hypoperfusion-induced demye-lination and clarified SNPH as a promising target in the treatment of hypoxic-ischemic forms of demyelination.

Introduction

Ischemic/hypoxic lesions, which frequently caused by modest but chronic hypoperfusion or sometimes acute ischemia in the brain, has been reported to cause injuries on myelinated axons in the white matter. Although intact myelin is an important site to ensure the functional spread of electrical impulses that propagate along with the myelinated fibre, the mechanisms underlying demyelination have been rarely investigated in the ischemic-hypoxic demyelination models.

In hypoxic-ischemic forms of demyelination, loss of oligodendrocytes has been noticed and obvious axonal injuries have also been reported by other studies[1, 2]. Unlike immune-mediated demyelinating diseases (e.g. multiple sclerosis, MS), in which myelin and oligodendrocytes are believed to be the primary targets and axonal injury is regarded as a secondary event to the myelin damage[3], it remains unclear which injury is the primary events and subsequently influenced the other pathological changes in hypoxic-ischemic demyelination.

The paranode regions of nodes of Ranvier are where axo-glial junctional complexes anchor the myelin sheath to the axon, and breakdown of paranodal complexes facilitates demyelination [4, 5]. Myelin degeneration in the paranode due to autoimmune reactions to the nodes/paranodes has been reported in

inflammatory peripheral neuropathies[6, 7]. However, the stability of paranodal complexes in the hypoxic-ischemic forms of demyelination in the central nervous system has not been examined.

Under hypoperfusion, neurons are vulnerable to ischemic/hypoxic insults, with mitochondria act as quick-response organisms. Mitochondria in the axon's manifest various changes, such as abnormal antegrade and retrograde movements, mitophagy or generating reactive oxygen species (ROS)[8, 9]. Although the function of these dynamic changes is not thoroughly understood, the mitochondrial malfunction has been reported to be involved extensively in the development of immune-mediated demyelination[10, 11]. SNPH, as an axonal specific protein, can tether and immobilize axonal mitochondria to microtubules at stationary sites. And the release or anchoring of mitochondria by SNPH have been proved to influence the progression of many demyelination diseases. Thus, it is reasonable to speculate that axonal mitochondrial dynamics may be involved in hypoxic-ischemic forms of demyelination. In this study, using a bilateral common carotid artery stenosis (BACS) mouse model and an in vitro cerebellum slice model treated with Low glucose-low oxygen (LGLO), we attempted to investigate the relationship between axon injuries, paranode stability and demyelination, as well as the role of mitochondria, especially the SNPH-mediated immobilization of mitochondria in the development of hypoxic-ischemic forms of demyelination.

Methods

Animals

C57BL/6J male mice (6-8 weeks, 20-25 g) were purchased from Charles River and housed in the Experimental Animal Center of Fudan University in a temperature and humidity-controlled specific-pathogen-free laboratory with a 12 h/12 h light/dark cycle. All procedures were performed in accordance with the Guide for the National Science Council of the People's Republic of China, and the study was approved by the Ethics Committee of Fudan University, Shanghai, China (IRB approval number 20180972A259). This manuscript was written in accordance with the Animal Research: Reporting of In Vivo Experiments (ARRIVE) guidelines.

BCAS model and experimental design

The BCAS model was created as previously described[12]. Briefly, mice were anaesthetized using 4% isoflurane in 30% O_2 and 70% N_2 and maintained on 2% isoflurane in 30% O_2 and 70% N_2 using a mask. A midline skin incision was made, and the bilateral common carotid arteries were isolated and subsequently stenosed using 0.18 mm steel micro coils (Wuxi Samini/Sawane Spring Co., Ltd.; Hamamatsu City, Japan). For sham-operated mice, a similar procedure was followed, but micro-coils were not used for BCAS induction.

All the experimental groups were randomized, and all the outcome analyses were carried out by independent investigators blinded to the treatment conditions and mouse types. Randomization of each

experimental group was performed before the surgical procedure using the random number generator in GraphPad. For TEM and the eight-arm maze experiments, preliminary data indicated that six and twelve animals per group, respectively, would suffice to obtain 80% power at a significance level of <0.05 with a two-sided test.

Cerebellum slice culture and experimental design

Cerebellar organotypic slice culture from postnatal day 8-9 (P8-9) mice were used to investigate hypoperfusion-induced demyelination. Briefly, 400 μm P8-9 mouse cerebellum parasagittal slices were obtained using a Tissue Slicer (ZQP-86; Zhixin Co., Ltd.; Shanghai, China). The slices were placed on cell culture inserts (Millipore, Bedford, MA, USA) and cultured in 50% DMEM with 25% HBSS, 25% horse serum, and 5 mg/ml glucose (Invitrogen, Carlsbad, CA, USA) in cell culture chambers at 37 °C.

Oxygen and glucose deprivation is a classic model for studying tissue ischemic responses to mimic the whole brain hypoperfusion, we used modified low glucose and low oxygen (LGLO) treatment for 48 h. Experiments and data analyses were performed in a double-blinded manner.

SNPH shRNA and AAV. SNPH-shRNA construction and stereotactic injection

shRNA targeting SNPH (Nosc-41370-SH, Santa Cruz Biotechnology, USA) was transfected using Lipofectamine 3000 (Invitrogen) according to the manufacturer's instructions. 72 h after transfection, slices were processed for LGLO treatment. Western-blotting and immunostaining were subsequently performed for further analysis.

We further used the shRNA bought from Santa Cruz Biotechnology to synthesize the AAV. SNPH-shRNA with the hSyn promoter (GeneChem, Shanghai, China), and the synthesized AAV. SNPH-shRNA or AAV. control-shRNA was stereoscopically injected into lateral ventricles. Briefly, mice were anaesthetized using 4% isoflurane in 30% O_2 and 70% N_2 and maintained on 2% isoflurane in 30% O_2 and 70% N_2 using a mask. AAV vectors were infused into the left lateral ventricle (coordinates from bregma: AP, −0.2 mm; ML, +1.0 mm; DV, −2.3 mm). 5×10^{11} genome copies were infused at a rate of 4 μl min^{-1}, after which the needle was left in place for 2 min to prevent backflow before the withdrawal.

SNPH overexpression lentivirus construction and administration

SNPH overexpression plasmid and lentivirus was constructed by Genomeditech (Genomeditech, Shanghai, China). Lentivirus was added to the slice medium at 1*108TU/ml 72 h before LGLO treatment. Western blotting and immunofluorescence were subsequently performed for further analysis.

Time-lapse imaging using confocal microscopy

Mitochondria were labelled with CMXRos after brain slices were treated with LGLO. The distribution, size, and mean transport velocity of CMXRos-positive mitochondria in myelinated and demyelinated Purkinje cell axons were imaged using the Olympus inverted confocal microscope as described previously[2].

Briefly, 3 h before imaging, slice medium containing 100 nM Mito Tracker (M7512, ThermoFisher, USA) was added to the slice chambers. Then, slices were washed thrice in PBS and replenished with normal culture medium for further live imaging in an airstream incubator at 37 °C using a 60x 1.3 NA oil immersion objective with 512 x 512-pixel resolution.

Upon imaging, a total of 5 min with 5s intervals were imaged for each experiment. Total live imaging time was restricted to 20 min to minimize phototoxic damage. Lengths, areas, and diameters of axonal mitochondria were measured by ImageJ (NIH, USA). The number and mean velocity of motile mitochondria were analyzed by kymographs. Stationary sites in this study were defined as CMXRos-positive profiles that were stationary during a 5-min period. To measure the size of the stationary sites, a pair of image stacks, including all CMXRos-positive profiles of each axon, were obtained at time 0 and time 5 min.

Immunofluorescence

Brain slices were fixed overnight in PBS containing 4% formaldehyde and then in 30% sucrose for 2 days at 4 °C. For cultured neurons grown on polylysine (PLL) coated glass, cells were blocked with PBS containing 5% BSA for 1 h after three washes with PBS and permeabilization with 0.1% Triton X-100 in PBS for 15 min. Primary antibodies diluted in blocking buffer were added and incubated at 4 °C overnight. We used anti-NF (1:50, ab8135, Abcam, USA), anti-MBP (1:200, ab40390, Abcam, USA), anti-Caspr (1:100, ab252535, Abcam, USA), anti-Nav1.6 (1:200, ASC-009, Alomone Labs, Israel), and anti-panNfasc (1:100, MABN621, Sigma Aldrich, USA) antibodies. Slices were washed with PBS three times and labelled with a fluorescence-conjugated secondary antibody for 1 h (Alexa Fluor 488 and 594, 1:1000, Life Technologies). Nuclei were visualized with DAPI (28718-90-3; Sigma Aldrich, USA).

For ROS staining, MitoSOX™ Red mitochondrial superoxide indicator (M36008, ThermoFisher, USA) was used to label ROS in mitochondria. Briefly, MitoSOX was diluted according to the manufacturer's instruction and incubated with the slices for 3 h. Thereafter, the slices were washed with PBS three times and replenished with the indicated culture medium. After LGLO treatment, slices were fixed with 4% formaldehyde overnight and 30% sucrose for 2 days at 4 °C. Subsequent immunostaining was performed as described above.

Western blot

Brain slices were collected and lysed in RIPA buffer (50 mM Tris-HCl, pH 7.5, 150 mM NaCl, 1% Triton X-100, 0.1% SDS, 0.5% deoxycholate) with protease inhibitor. Equal amounts of proteins measured using the BCA method were loaded and analyzed after 15% Bris-Tris NuPAGE and then transferred onto nitrocellulose membranes. The membranes were incubated overnight at 4 °C with following primary antibodies: anti-SNPH (ab69992, Abcam), anti-Miro1 (ab188029, Abcam), anti-Trak1 (ab28751, Abcam), anti-HSP60 (ab190828, Abcam), anti-Caspr (ab216144, Abcam), anti-MBP (ab77924, Abcam), anti-NF155 (ab186734, Abcam), and anti-β -actin (ab115777, Abcam) at a dilution of 1:1000.

Transmission Electron Microscope

Transmission electron microscope (TEM) was performed as previously described[13]. In brief, brain samples were perfused with 4% formalin and fixed in formalin overnight. Dissected tissues (1 mm in thickness) were post fixed in buffered OsO_4, dehydrated in graded alcohol solutions and propylene, embedded in Epon, and examined by light microscopy after toluidine blue staining. Thin sections cut on formvar-coated slot grids and stained with uranyl acetate and lead citrate were examined using a JEOL 1200 electron microscope. G ratios were determined as the inner to outer axonal circumference ratio using ImageJ.

Eight-arm radial maze test

The eight-arm radial maze test was performed as previously described[14]. The maze consisted of a central platform (24 cm in diameter) with eight arms that extended radially. Rats were allowed to visit each arm to eat eight pellets in food cups placed near the end of each arm. Each test animal was trained once per day to memorize the apparatus. The performance of test animals in each trial was assessed using two parameters: number of correct choices in the initial eight chosen arms and number of errors (defined as choosing arms that had already been visited). When the test animals made seven or eight correct choices and no more than one error in three successive sessions, they were deemed to have memorized the maze.

Whole-cell patch-clamp electrophysiology

Cultured brain slices were transferred to the bath solution for 1 h prior to recording. The bath solution contained 126 mM NaCl, 2.5 mM KCl, 26 mM , 1.25 mM , 2 mM , 2 mM , and 11 mM glucose was bubbled with 95%+5%; the temperature of bath solution was maintained at 35 °C. For mEPSC recordings, patch pipettes contained 126 mM K-gluconate, 4 mM KCl, 4 mM ATP-Mg, 0.3 mM GTP-, 10 mM PO creatine, 10 mM HEPES, and 0.2-0.5% biocytin (pH 7.3 adjusted using KOH, 300 mOsm maintained using sucrose) with a tip resistance of 6–8 MΩ. During mEPSC recording, TTX (0.5 μM), was administered to silence network activity through inhibition of voltage-sensitive sodium channels, and bicuculline (10 μM) was given to block the $GABA_A$-mediated inhibitory signalling.

For APs recording, patch pipettes contained 140 mM K-gluconate, 5 mM EGTA, 0.5 mM , 2mM ATP-Mg, 0.3 mM GTP-, 10mM sucrose, 10mM HEPES, and 0.2-0.5% biocytin (pH 7.3 adjusted using KOH, 300 mOsm maintained using sucrose) with a tip resistance of 6-8 MΩ.

Series resistance was monitored in 2 min intervals, and recordings were excluded if the series resistance and leak current changed significantly and/or exceeded 40 MΩ or 200 pA, respectively.

Cerebral blood flow measurement

Cerebral blood flow measurement was performed as previously described[15]. Briefly, mice were anaesthetized using 4% isoflurane in 30% O_2 and 70% N_2 and then maintained on 2% isoflurane in 30%

O_2 and 70% N_2 using a mask. The temperature of the animals was maintained at 37 °C using a heating pad and a feedback control system (FHC; Bowdoin, ME, USA). A midline incision was made on the skin of the skull, and a laser Doppler probe was fixed in place (5 mm lateral and 2 mm posterior to the bregma). Each measurement was repeated three times.

Statistical analysis

Data were analyzed using SPSS Statistics 20 and graphed with GraphPad Prism 6.0. The sample size was calculated based on power as 0.95 and α as 0.05. All the data from mice are represented as the mean ± SD and data from brain slides are represented as mean ± SEM. Different treatment groups were evaluated using one-way analysis of variance (ANOVA) with Tukey's test for multiple comparisons or two-way ANOVA to determine differences among individual groups. The null hypothesis was rejected when P-value was <0.05.

Results

1. **SNPH-mediated mitochondrial accumulation in axons was an early event that preceded hypoperfusion-induced demyelination and cognitive impairment**

In order to explore the relationship of the mitochondria dynamics and demyelination pathological changes in axon after hypoxia-ischemia injury, BCAS mouse model was used to induce whole-brain low perfusion[16]. After coils were placed around the bilateral common carotid arteries, reduced cerebral blood flow was observed in the anterior circulation area and lasted for at least 28 days (Fig. S1a). Cognitive impairment was also observable at day 28 after BCAS (Fig. S1b-d), demonstrating that the BCAS model was qualified. Using this model, we were able to acquire brain sections at different stages after hypoperfusion and observe the ultrastructure of myelin as well as the relationship with mitochondria using TEM. As expected, we observed obvious demyelination in the corpus callosum at day 28 after BCAS, instead of day 7, indicating that the demyelination is increasingly growing after BCAS (Fig. 1a, b, c). Interestingly, we observed a robust increase in the number of mitochondria with increased length and decreased diameter per axonal area in the corpus callosum at day 28 after BCAS (Fig. 1d, e, f), showing that the changes of mitochondria in axons were closely related to demyelination. It was noteworthy that mitochondrial accumulation occurred as early as 7 days after BCAS, while demyelination was not yet observable (Fig. 1a-d), implying that mitochondrial accumulation in axons precedes hypoperfusion-induced demyelination.

Since mitochondrial accumulation is mainly regulated by the mitochondrial transport machinery, we then assessed the levels of proteins related to mitochondria movement. Levels of Miro (Miro1) and Milton (Trak1), the major motor adaptors which mediate mitochondrial motility, did not change after BCAS; however, levels of the major mitochondrial docking protein, SNPH, were significantly increased at day 7 after BCAS and remained elevated till day 28 after BCAS (Fig. 1g, h), indicating that SNPH may serve as a major mediator of mitochondrial accumulation and demyelination in the hypo-perfused axons.

To investigate the participation of SNPH in the development of hypoperfusion-induced demyelination, we employed an adeno-associated virus (AAV) stereotype 9 vectors, encoding SNPH-shRNA under the control of the hSyn promoter, which can specifically transfect neuronal cells (Fig. S1e, f, g). We observed that mitochondrial load per axonal area was reduced and abnormal mitochondrial morphology was also recovered by SNPH knockdown after 28 days of BCAS (Fig. S2a, b, c). Consistently, hypoperfusion induced demyelination was partially rescued by SNPH knockdown, as shown by the improvement of myelin structure and a significant drop in the elevated G ratio after 28 days of BCAS (FigS2. d-g).

2. **Paranode instability accompanied by axonal mitochondrial accumulation reveals early changes preceding hypoperfusion-induced demyelination**

To further investigate the correlation between mitochondria accumulation and demyelination as well as the timeline of these two processes in axons after BCAS, we next observed the paranodal ultrastructure of the node of Ranvier. Paranodal region is where myelin sheath anchors to the axon, flanking to the node of Ranvier and is vital for maintaining intact and functional myelin. The myelin sheath (oligodendroglia) attaches to the axon by forming a spiral junction in the paranodal region, which has the appearance of a series of loops. Thus, the paranodal junctions are characterized by evenly spaced, transverse bands connecting the glial membrane to the axolemma[17]. Using TEM, we observed that mitochondria with clear and sharp cristae were evenly distributed in axons in the sham group. Paranodal loops adhered tightly to axons via the transverse bands, and myelination was tight and intact (Fig. 2a). At day 7 of BCAS, the mitochondrial load in axons was increased, but mitochondrial morphology was intact and normal; paranodal loops had started to disengage from the axonal surface, and increased transverse bands were observed, but myelin sheath was still intact (Fig. 2a-d). At day 14 of BCAS, mitochondria showed an elongated and swollen appearance with broken cristae, and these elongated mitochondria were accumulated even more robustly in axons. Detached paranodal loops were evident as cytoplasm filled wraps of uncompacted myelin. Demyelination was also obvious as a significant reduction in the G-ratio (Fig. 2a-d). At day 28 of BCAS, broken mitochondria with a severely swollen appearance were predominantly accumulated in axons. The paranodal loops and paranodal junctions were dramatically damaged, and demyelination had progressed even further as evidenced by myelin loss along axons (Fig. 2a-d). From above, it was clear that axonal mitochondrial accumulation occurred prior to demyelination, which was accompanied by a loss of paranode integrity. We speculated that mitochondrial accumulation/dysfunction occurred at a very early stage of hypoperfusion might gradually induce myelin damage through impairing the paranodal ultrastructure.

Next, we attempted to find how mitochondrial accumulation deteriorated paranode instability. In the paranodal segments, oligodendroglia anchors to axon by paranodin/Caspr/Nf155 complex. Axonal paranodin/Caspr and the oligodendroglial adhesion molecule Nf155 form septate-like junctions, anchoring myelin loops to axons[18]. The integrity of the paranodin/Caspr/Nf155 complex ensures intact paranodal structure and functional myelin. Therefore, we hypothesized that mitochondrial accumulation

in axons might initially impair the stability of the paranodin/Caspr/Nf155 complex. Indeed, we found that Caspr and Nf155 levels were significantly reduced at 7 days after BCAS, whereas myelin basic protein (MBP), a specific marker of myelin, was unchanged (Fig. 2e, f). The levels of Caspr and Nf155 kept reducing to day 28, and MBP showed a decrease from day 14 to day 28 (Fig. 2e, f). These results were consistent with the ultrastructural changes observed using electron microscopy (Fig. 2a-d), supporting the hypothesis that accumulated axonal mitochondria impaired paranode structure in the very early stages of hypoxia and then induced demyelination.

Using a panNfasc antibody to label the Nf155 and Nf188 complex, we further assessed the integrity of the paranode structure using confocal microscopy. The co-localization of Caspr and panNfasc signals indicates the integrity of the paranode structure, and we found a significant reduction in the co-localization of Caspr and panNfasc signals within the paranodes at day 7 post-BCAS, suggesting that a breakdown in the paranode structure. Moreover, this reduction lasted till day 28 after BCAS (Fig. 2g and h). Voltage-gated sodium channels, such as Nav1.6, on the nodes of Ranvier, are important sites for action potential propagation and are physically flanked by myelinated axon segments[19]. A significant increase of the length of Nav1.6 was observed from day 14 to day 28, but not on day 7, further supporting that accumulated mitochondria impair paranode structure earlier than pathological demyelination of axons (Fig. 2g, i).

3. SNPH-mediated mitochondrial accumulation exacerbates demyelination by impairing paranode stability

The above results revealed that axonal mitochondrial accumulation, which related to neuron-specific mitochondrial anchoring protein SNPH, was the initial factor for paranode instability after hypoperfusion. Therefore, we investigated whether the lack of SNPH would exert initial protective effects on paranodes by improving mitochondrial dynamics in axons. Using SNPH shRNA to knockdown SNPH, we found that the accumulation of mitochondria was mitigated and paranode structure was improved at day 7 of BCAS (Fig. 3a-d). At day 28 of BCAS, SNPH knockdown significantly mitigated mitochondrial accumulation in axons and alleviated the swollen morphology. Impairment of paranode stability and demyelination was also rescued by SNPH knockdown (Fig. 3a-d). Consistent with the ultrastructural changes, Caspr and Nf155 (Fig. 3e, f) expression and colocalization of Caspr and panNfasc were decreased on both day 7 and day 28 of BCAS (Fig. 3g, h). The length of Nav1.6 was increased on day 28 (Fig. 3g, i). However, diminished Caspr, Nf155, MBP expression, decreased colocalization of Caspr and panNfasc signals, and increased length of Nav1.6 were all rescued by SNPH knockdown (Fig. 3e-i). Together, these observations demonstrated that after chronic hypoperfusion, SNPH knockdown reduced the accumulation of mitochondria in axons and promoted paranode stability at an early stage and subsequently mitigated demyelination at a late stage.

4. **SNPH knockdown stabilizes paranodal structure through promoting mitochondrial movement and reducing mitochondrial ROS production**

To further clarify the mechanisms of SNPH knockdown in regulating paranode instability and demyelination, we established an in vitro model of hypoperfusion-induced demyelination in cerebellum slice cultures maintained in chronic low oxygen and low glucose (LGLO) conditions. As a mitochondrion arching protein, we first speculated that the effects of SNPH knockdown might be related to mitochondrial dynamics. As shown by MBP immunostaining, LGLO treatment successfully induced demyelination at 48 h (Fig. S3a-d). Next, we analyzed axonal mitochondrial distributions and transport after LGLO treatment (Fig. S3e). Mitochondrial load in axons was significantly higher after 12 h of LGLO treatment and was doubled at 48 h, along with an increase in mitochondrial size (Fig. S3f, g). In addition, the proportion of stationary mitochondria was dramatically increased after 12 h of LGLO treatment (Fig. S3h). Consistently, both anterograde and retrograde transport of mitochondria decreased after 48 h, with elevated levels of SNPH under LGLO treatment (FigS3. i and j). These results were insistent with what we observed in vivo in BCAS mice after 7 days and 28 days. To down-regulate SNPH in this model, cerebellum slices were transfected with SNPH-shRNA (Fig. S4a, b). SNPH-knockdown caused a robust increase in both anterograde and retrograde transport in LGLO treated axons (Fig. 4a, b). Moreover, mitochondrial load and size in axons were significantly decreased (Fig. 4 c, d), indicating that enhanced mitochondrial transport by SNPH knockdown reduced the mitochondrial accumulation in axons.

Impaired transportation of mitochondria and mitochondrial overload in axons exerts harmful effects on neurons, especially in terms of disrupted clearance of malfunctioning mitochondria by retrograde transport[20], because malfunctioning mitochondria can produce ROS in axons under hypoxic conditions[21, 22]. ROS was reported to be detrimental to the paranode structure, specifically the Nf155/paranodin/Caspr complex[23]. To test whether SNPH knockdown could reduce ROS generation in axons, MitoSOX was used to label mitochondrial ROS production. We found that 48 h of LGLO treatment induced significant elevation of mitochondrial ROS levels not only in cell bodies but also in the axons (Fig. 4e). However, SNPH knockdown alleviated the mitochondrial ROS production in axons and also reduced overall ROS production (Fig. 4e, f, g). Impaired MBP expression and structural changes induced by LGLO treatment were also partly rescued by SNPH knockdown (Fig. 4h-k). These results suggest that SNPH knockdown improved demyelination by promoting mitochondrial transport and might by reducing ROS production.

To further verified that elevated mitochondrial ROS levels in axons could cause deterioration of the demyelination pathology, we overexpressed SNPH using a lentiviral vector in cerebellum slice cultures (Fig. S4c, d). Together, we adopted MitoQ10, a selective mitochondrial ROS inhibitor, to inhibit mitochondrial ROS production. Results showed that SNPH overexpression significantly elevated mitochondrial ROS production in axons (Fig. 5a, b, c). In addition, Caspr and NF155 expression was reduced and the colocalization of Caspr and panNfasc was impaired in SNPH overexpressed tissue (Fig. 5d-g). With MitoQ10 treatment, mitochondrial ROS level elevation was mitigated (Fig. 5a, b, c). Accordingly, Caspr and NF155 expression was increased and the colocalization of Caspr and panNfasc

was also rescued (Fig. 5f, g), indicating that ROS from overloaded stationary mitochondria destabilized paranode structure.

Thus, we concluded that mitochondrial overload in axons was able to serve as an initiation factor and triggered ROS production, which then impaired paranodal structure and led to demyelination. This also explained our observation in BCAS/LGLO-induced neurons where demyelination could be ameliorated by SNPH knockdown.

5. **SNPH knockdown promotes synapse activity and enhanced cognitive function**

Insufficient perfusion often leads to hampered neuron excitability and subsequent cognitive impairment or other neuronal malfunctions[24, 25]. A previous study has identified the pivotal role of anterograde mitochondrial transport in providing sufficient energy for functional synapse signaling[26]. Besides, intact myelin is important for the transmission of action potentials. Based on the above findings, impaired anterograde transport was improved, and demyelination was alleviated by SNPH knockdown in the LGLO model/BCAS mice, it was reasonable to speculate that SNPH knockdown may rescue neuronal function.

To evaluate the changes in neuron excitability, the whole-cell patch-clamp method was used. First, we examined the intrinsic excitability of Purkinje neurons measured as the number of action potentials elicited by a given current injection（Fig. 6a). 48 h of LGLO treatment resulted in a remarkable drop in firing rate at all injection amplitudes, accompanied by a loss in neuron input resistance (Fig. 6b). Compared to the control, the largest drop in firing rate was observed with the smallest current injections, indicating that LGLO treatment mostly affected firing rates at membrane potentials that were relatively close to resting membrane potential (Fig. 6c). However, in SNPH knockdown neurons, intrinsic excitability showed an obvious recovery, followed by an increase in input resistance (Fig. 6a-d).

Next, we assessed synapse signalling after LGLO treatment. Both miniature excitatory postsynaptic current (mEPSC) amplitude and frequency decreased dramatically after LGLO treatment, whereas mEPSC amplitude and frequency were increased when SNPH was knockdown (Fig. 6e, f, g). Cumulative mEPSC distribution curve analysis showed that SNPH knockdown built up a significantly more abundant mEPSC amplitude and smaller inter-mEPSC intervals (Fig. 6h, i).

Moreover, we texted the behaviour of BCAS mice with/without SNPH knockdown. Working memory was impaired in BCAS mice, but this impairment was reversed by SNPH knockdown, as evidenced by subsequent improvement in revisiting errors (Fig. 6j). In addition, the number of different arm choices in the first eight entries showed that BCAS mice performed worse than sham-operated mice in each successive training session, whereas SNPH knockdown mice performed better (Fig. 6 k, l). Collectively, these data indicate that SNPH knockdown promotes synaptic function and overall neuron excitability, which also benefit cognition.

Discussion

In this study, we found that axonal insult was the primary event that subsequently impaired myelination in hypoxic-ischemic demyelination, which was distinct from inflammatory demyelination that immune system attacks myelin at the first place. The negative influence of axonal insult on demyelination in hypoxic-ischemic demyelination was mainly through impairing the paranode stability, which is a critical place for myelin to anchored on the axons. The extensive accumulation of mitochondria among axons produced unfavourable ROS which interfered the connection of Nf155 and Caspr within the paranode and subsequently mediated the axonal influence on paranode stability. We further revealed that the elevated SNPH was responsible for the accumulation of mitochondria in axons. SNPH knockdown significantly mitigated the accumulation of mitochondria and ROS production, rescued the paranode impairment and alleviated demyelination and cognitive impairment in vivo and in vitro. To our knowledge, this study is the first to clarify the extensive mechanistic involvement of the impairment of mitochondrial dynamics in the development of hypoxic-ischemic demyelination and implicates SNPH as a specific therapeutic target which may help mitigate this dysfunction.

The pathological process of inflammatory demyelination involves peripheral autoimmune activation, multifocal inflammation, demyelination and subsequent axonal degeneration[27]. Inflammatory demyelination usually results from a combination of humoral and cellular autoimmunity, which attack structural proteins of compact myelin. Autoimmune antigenic targets such as T cells and MOG in MS, aquaporin-4 in neuromyelitis optical, or autoantibodies against antigens (including Caspr1, contactin-1, Nf155, et.al) at the node of Ranvier cause demyelination or axonal degeneration[27]. However, for the hypoxic-ischemic forms of demyelination, which usually occurs in patients with small vessel cerebrovascular disease, global brain hypoxia, leukoaraiosis or even stroke, is thought to be caused by either modest but chronic shortage of oxygen and nutrient supply through chronic hypoperfusion of the white matter or a severe attack from focal ischemia which involves white matter[28]. This kind of demyelination often results from a form of incomplete infarct or selective necrosis, sometimes results from occlusion of small penetrating arteries that selectively perfuse subcortical white matter areas or fibre tracts. The pathological process of this kind of demyelination includes intramyelinic oedema that manifests as myelin pallor, further vacuole formation and sheath destruction followed by myelin debris clearance by microglia and macrophages[29]. During this process, hypoperfusion not only affects oligodendrocytes but also neurons and glia cells, involving the interaction between cells.

It is well known that neurons are highly sensitive to hypoxia and ischemia and neurons response as early as few minutes to ischemia. Glutamate excitotoxicity, mitochondrial dysfunction, oxidative stress and proinflammatory factors from injured neurons act as exacerbation factors, which might influence the oligodendrocyte directly because they are next to each other structurally. Thus, more attention should be paid on the effects of neurons on myelin after chronic hypoxia. Our results indicate that neuronal cells are more vulnerable to hypoxia-ischemic condition and neuronal dysfunction happens preceding demyelination as proved by the excessive accumulation of mitochondria among axons at an early stage of BCAS and subsequent alleviation of demyelination by decreasing the load of mitochondria among

axons. Therefore, contradict to inflammatory demyelination which focusing on immune insult on myelination, axonal influence on hypoxic-ischemic demyelination should be taken seriously and could be a potential therapeutic target to mitigate demyelination and cognitive impairment.

The structural connection of axon and oligodendrocytes is the nodes of Ranvier. Nodes of Ranvier mediate saltatory conduction in axons in CNS, consisting of three domains: the node, the paranode and the juxtaparanode[18]. Each of these domains has a distinct molecular architecture, with a large number of channels, structural proteins and adhesion molecules[30]. The most important characteristic of paranode is the presence of axoglial septate-like junctions, which attach the myelin loops to the axon. The loss or damage of normal paranode structure contributes to demyelination. Following the clues of axonal influence on demyelination, we then focused on the paranode structure changes after BCAS. For the first time, we report here that paranode stability dropped in accord with axonal mitochondria accumulation and the alleviation of this abnormal accumulation substantially protected the paranodal stability. The paranode stability relies on adhesion molecules that mediate axoglial attachment. The main molecules, such as Nf155, Caspr1 and Contactin1, also called paranode complex[31]. When we examined the expression of paranode complex proteins, we observed similar changes, shown as decreased Nf155 and Caspr1 levels in accord with axonal mitochondria accumulation and the alleviation of this abnormal accumulation substantially reversed their levels and structural integrity.

It has been reported that paranode stability is sensitive to ROS[32]. However, whether the destroy of paranode comes from axonal ROS due to the accumulated mitochondria has not been studied. Through labelling the ROS production in axonal mitochondria, we found the consistency of mitochondrial ROS production and subsequent elimination of paranodal junction protein such as Nf155 and Caspr, as well as myelin loss. The demyelination and the loss of paranodal junction protein could also be rescued by blocking the production of mitochondrial ROS. In conclusion, our research is mainly focusing on the relationship between the paranode structure and hypoxic-ischemic forms of demyelination and proved that damage of paranode structure is prior to demyelination. The axonal mitochondria accumulation in hypoxic-ischemic demyelination deteriorated the paranode stability through excessive ROS production and served as a preceding event to significantly influence the progression of demyelination.

In order to alleviate abnormal accumulation in axons after BCAS/LGLO, we adopted a virus-based SNPH knockdown technique. SNPH is an axonal specific protein that tethers and immobilizes axonal mitochondria to microtubules at stationary sites[33]. And the release or anchoring of mitochondria by SNPH have been proved to influence the progression of many demyelination diseases[34]. For example, in an MS model (Shiverer mice), SNPH-mediated anchoring of mitochondria among axons was increased, which provide sufficient metabolic demands for axons to survive at very early stage[34]. But the excessive anchoring of mitochondria prevents the replenishment of fresh mitochondria from soma to axon and also inhibits the replacement of malfunctioned mitochondria by mitophagy, thus improper responding to the chronic stress environment leads to deteriorated demyelination by excessive ROS expression and mismatch of ATP[34]. In another study using MS model, when SNPH was overexpressed in dendrites,

Purkinje cells showed compromised neuronal viability by inducing N-methyl-D-aspartate (NMDA) excitotoxicity, reducing mitochondrial calcium uptake, and degrading mitochondrial quality by impeding somal mitophagy[35]. Although accumulated mitochondria and demyelination is reduced when SNPH is knockdown, however, in and hypoxic-ischemic forms of demyelination, the role of SNPH in mitochondrial dynamics and cell function is still unclear.

Mitochondrial transport underlies the mitochondria distribution and influences the cell function. Anterograde transport replenishes fresh mitochondria necessary for synaptic function, and retrograde transport enables the clearance of malfunctioning mitochondria for mitophagy[36, 37]. Since both the anterograde and retrograde transport of mitochondria was observed upon SNPH knockdown, we hypothesized that SNPH knockdown improves the function of axons and neurons. Our results indicate that ROS production could be elevated by increasing the anchoring of mitochondria by SNPH and it further impaired the paranode stability. More importantly, we revealed that improved retrograde transport of mitochondria is critical to mitigating mitochondrial ROS production which could significantly protect the paranodal stability upon SNPH knockdown. Therefore, SNPH elevation reasonably accounted for pathology and disease progression of hypoxic-ischemic demyelination.

Next, we separately investigated neuron excitability by SNPH knockdown. Neuron excitability relies on the intact structure of Nodes of Ranvier and myelin, as well as the fresh mitochondria transport to axon for ATP supply. Since we observed both mitigated demyelination and improved anterograde transport by SNPH knockdown, we expected to see the improvement of neuron excitability. This hypothesis is supported by our results that a remarkable drop in firing rate accompanied by a loss in neuron input resistance was observed under LGLO, however, in SNPH knockdown neurons, both intrinsic excitability input resistance was recovered. In addition, synapse function was improved when SNPH was knockdown, shown as both mEPSC amplitude and frequency decreased after LGLO treatment, whereas both were increased upon SNPH knockdown.

Because ischemia usually results in cognitive impairment primarily due to the reduction in cerebral blood flow, we further examined this beneficial effect on the behaviour of SNPH knockdown in vivo and observed improved working memory in the BCAS model. Collectively, improved synaptic function and enhanced mitochondrial ROS clearance were observed after SNPH knockdown, which indicated that replenishment and clearance of mitochondria are necessary for normal neuronal function in hypoxic-ischemic demyelination. Until now, no FDA-approved drugs have been developed to mitigate hypoxic-ischemic demyelination, but the number of patients suffering from reduced quality of life and heavy living expenses due to hypoxic-ischemic demyelination is increasing[38]. Thus, there is an urgent need to uncover the mechanism of hypoxic-ischemic demyelination and to design appropriate and optimal therapeutic strategies. Here, we discovered the necessary and sufficient role of SNPH in the development of hypoxic-ischemic demyelination, which makes it a promising therapeutic target for further drug development.

In conclusion, our results indicate a distinctive pathological characteristic of hypoperfusion-induced demyelination that axon insult happens preceding demyelination. The elevated expression of SNPH in hypoxic-ischemic demyelination in vivo and in vitro leads to the accumulation of mitochondria among axons. SNPH-mediated immobilization of mitochondria mediates the detrimental effect of axon dysfunction and paranode instability through ROS production among axons. Knockdown of SNPH alleviates mitochondria load among axons and promotes anterograde and retrograde mitochondria transport stabilized paranode structure and rescued the hypoxia-induced demyelination. Our results provide a novel insight into the pathological changes under hypoperfusion and identified SNPH as a therapeutic target to mitigate the development of hypoxic-ischemic demyelination.

Abbreviations

AD, Alzheimer's' disease; APs, Action potential; BCAS, Bilateral common carotid artery stenosis; LGLO, Low glucose-low oxygen; mEPSC, Miniature Excitatory Postsynaptic Current; MS, Multiple sclerosis; ROS, Reactive oxygen species; SNPH, Syntaphilin; TEM, Transmission electron microscopy; VaD, Vascular dementia.

Declarations

Ethics approval

All procedures were performed in accordance with the Guide for the National Science Council of the People's Republic of China, and the study was approved by the Ethics Committee of Fudan University, Shanghai, China (IRB approval number 20180972A259). This manuscript was written in accordance with the Animal Research: Reporting of In Vivo Experiments (ARRIVE) guidelines.

Consent for publication

All authors have approved of the contents of this manuscript and provided consent for publication.

Availability of data and materials

The datasets used and/or analyzed during the current study are available from the corresponding author on reasonable request.

Competing interests

There are no conflicts of interest to declare.

Funding

This study was supported by the National Natural Science Foundation of China (81971013 to M.C.; 81870915 and 81571109 to Q.D.), Grant from the Science and Technology Commission of Shanghai

Municipality (16411970200).

Author Contributions

YW and MG drafted the manuscript. YW and SD accomplished the experiment. YW and HC helped with statistics and figure preparation. MC and QD designed the experiment. All authors read and approved the final manuscript.

Acknowledgements

Not applicable

References

1. Wang, M. *et al.* Astrocytic connexin 43 potentiates myelin injury in ischemic white matter disease. *Theranostics* **9**, 4474-4493 (2019).

2. Washida, K., Hattori, Y. & Ihara, M. Animal Models of Chronic Cerebral Hypoperfusion: From Mouse to Primate. *Int J Mol Sci* **20**, 6176 (2019).

3. Friese, M.A., Schattling, B. & Fugger, L. Mechanisms of neurodegeneration and axonal dysfunction in multiple sclerosis. *Nature Reviews Neurology* **10**, 225-238 (2014).

4. Rosenbluth, J. Multiple functions of the paranodal junction of myelinated nerve fibers. *Journal of Neuroscience Research* **87**, 3250-3258 (2009).

5. Shepherd, M.N., Pomicter, A.D., Velazco, C.S., Henderson, S.C. & Dupree, J.L. Paranodal reorganization results in the depletion of transverse bands in the aged central nervous system. *Neurobiol Aging* **33**, 203.e213-224 (2012).

6. Vural, A., Doppler, K. & Meinl, E. Autoantibodies Against the Node of Ranvier in Seropositive Chronic Inflammatory Demyelinating Polyneuropathy: Diagnostic, Pathogenic, and Therapeutic Relevance. *Front Immunol* **9**, 1029-1029 (2018).

7. Roggenbuck, J.J., Boucraut, J., Delmont, E., Conrad, K. & Roggenbuck, D. Diagnostic insights into chronic-inflammatory demyelinating polyneuropathies. *Ann Transl Med* **6**, 337-337 (2018).

8. Misgeld, T. & Schwarz, T.L. Mitostasis in Neurons: Maintaining Mitochondria in an Extended Cellular Architecture. *Neuron* **96**, 651-666 (2017).

9. Suárez-Rivero, J.M. *et al.* Mitochondrial Dynamics in Mitochondrial Diseases. *Diseases* **5**, 1 (2016).

10. Campbell, G.R. & Mahad, D.J. Mitochondria as crucial players in demyelinated axons: lessons from neuropathology and experimental demyelination. *Autoimmune Dis* **2011**, 262847-262847 (2011).

11. Carvalho, K.S. Mitochondrial Dysfunction in Demyelinating Diseases. *Seminars in Pediatric Neurology* **20**, 194-201 (2013).

12. Nishio, K. *et al.* A mouse model characterizing features of vascular dementia with hippocampal atrophy. *Stroke* **41**, 1278-1284 (2010).

13. Takade, A. *et al.* Comparative studies of the cell structures of Mycobacterium leprae and M. tuberculosis using the electron microscopy freeze-substitution technique. *Microbiol Immunol* **47**, 265-270 (2003).

14. Satoh, Y. *et al.* Extracellular signal-regulated kinase 2 (ERK2) knockdown mice show deficits in long-term memory; ERK2 has a specific function in learning and memory. *The Journal of neuroscience : the official journal of the Society for Neuroscience* **27**, 10765-10776 (2007).

15. Liebert, A., Leahy, M. & Maniewski, R. Multichannel laser-Doppler probe for blood perfusion measurements with depth discrimination. *Medical and Biological Engineering and Computing* **36**, 740-747 (1998).

16. Venkat, P., Chopp, M. & Chen, J. Models and mechanisms of vascular dementia. *Exp Neurol* **272**, 97-108 (2015).

17. Nans, A., Einheber, S., Salzer, J.L. & Stokes, D.L. Electron tomography of paranodal septate-like junctions and the associated axonal and glial cytoskeletons in the central nervous system. *Journal of neuroscience research* **89**, 310-319 (2011).

18. Thaxton, C. & Bhat, M.A. Myelination and regional domain differentiation of the axon. *Results Probl Cell Differ* **48**, 1-28 (2009).

19. Caldwell, J.H., Schaller, K.L., Lasher, R.S., Peles, E. & Levinson, S.R. Sodium channel Na_v1.6 is localized at nodes of Ranvier, dendrites, and synapses. *Proceedings of the National Academy of Sciences* **97**, 5616-5620 (2000).

20. Lin, M.Y. *et al.* Releasing Syntaphilin Removes Stressed Mitochondria from Axons Independent of Mitophagy under Pathophysiological Conditions. *Neuron* **94**, 595-610.e596 (2017).

21. Murphy, M.P. How mitochondria produce reactive oxygen species. *Biochem J* **417**, 1-13 (2009).

22. Joshi, D.C. *et al.* Deletion of mitochondrial anchoring protects dysmyelinating shiverer: implications for progressive MS. *J Neurosci* **35**, 5293-5306 (2015).

23. Román, G.C. & Kalaria, R.N. Vascular determinants of cholinergic deficits in Alzheimer disease and vascular dementia. *Neurobiology of Aging* **27**, 1769-1785 (2006).

24. D'Haeseleer, M. *et al.* Cerebral hypoperfusion: a new pathophysiologic concept in multiple sclerosis? *J Cereb Blood Flow Metab* **35**, 1406-1410 (2015).

25. Picard, M. Mitochondrial synapses: intracellular communication and signal integration. *Trends Neurosci* **38**, 468-474 (2015).

26. Hollenbeck, P.J. Mitochondria and neurotransmission: evacuating the synapse. *Neuron* **47**, 331-333 (2005).

27. Stathopoulos, P., Alexopoulos, H. & Dalakas, M.C. Autoimmune antigenic targets at the node of Ranvier in demyelinating disorders. *Nat Rev Neurol* **11**, 143-156 (2015).

28. Pantoni, L. Cerebral small vessel disease: from pathogenesis and clinical characteristics to therapeutic challenges. *Lancet Neurol* **9**, 689-701 (2010).

29. Dewar, D., Underhill, S.M. & Goldberg, M.P. Oligodendrocytes and Ischemic Brain Injury. *Journal of Cerebral Blood Flow & Metabolism* **23**, 263-274 (2003).

30. Biederer, T., Kaeser, P.S. & Blanpied, T.A. Transcellular Nanoalignment of Synaptic Function. *Neuron* **96**, 680-696 (2017).

31. Kira, J.-i., Yamasaki, R. & Ogata, H. Anti-neurofascin autoantibody and demyelination. *Neurochemistry International* **130**, 104360 (2019).

32. Gruber, R.C. *et al.* The control of reactive oxygen species production by SHP-1 in oligodendrocytes. *Glia* **63**, 1753-1771 (2015).

33. Ohno, N. *et al.* Mitochondrial immobilization mediated by syntaphilin facilitates survival of demyelinated axons. *Proc Natl Acad Sci U S A* **111**, 9953-9958 (2014).

34. Joshi, D.C. *et al.* Deletion of mitochondrial anchoring protects dysmyelinating shiverer: implications for progressive MS. *The Journal of neuroscience : the official journal of the Society for Neuroscience* **35**, 5293-5306 (2015).

35. Joshi, D.C. *et al.* Inappropriate Intrusion of an Axonal Mitochondrial Anchor into Dendrites Causes Neurodegeneration. *Cell Rep* **29**, 685-696.e685 (2019).

36. Roger, A.J., Muñoz-Gómez, S.A. & Kamikawa, R. The Origin and Diversification of Mitochondria. *Curr Biol* **27**, R1177-r1192 (2017).

37. Neupert, W. & Herrmann, J.M. Translocation of proteins into mitochondria. *Annu Rev Biochem* **76**, 723-749 (2007).

38. Love, S. Demyelinating diseases. *J Clin Pathol* **59**, 1151-1159 (2006).

Supplementary Figure Captions

Fig. S1: Reduced cerebral blood flow and impaired working memory in BCAS mice model

a Quantitative analysis of cerebral blood flow in Sham and BCAS mice. One-way ANOVA with Tukey's correction. n=8 per group for each analysis. **b, c, d** Working and reference memory were assessed using the eight-arm maze test. Mice in BCAS 28d group showed more revisiting errors (**b**) and less different arm choices (**c**) compared with BCAS 7d and sham-operated mice. n=11 mice in each group. No impairment in spatial reference memory was observed between different groups (**d**). Two-way ANOVA for interaction factor $F_{6,120}$ = 14.33, p<0.0001 (**b**); $F_{6,120}$ = 12.02, p<0.0001 (**c**); $F_{16,240}$ = 3.780, p<0.0001 (**d**) with Dunnett's post-hoc test. **e, f** Representative immunoblot (**e**) and quantitative analysis (**f**) of SNPH expression in scr-shRNA and SNPH-shRNA treated mice. n=8 mice per group. Unpaired t-test, t=8.862, df=10, p<0.001. **g** Representative immunofluorescence images showing the transfection efficiency of SNPH-shRNA (green) in neuronal cells labelled using NeuN (red). Data are represented as means ± SD. (* p<0.05; ** p<0.01; *** p<0.001; ns: non-significant differences).

Fig. S2: SNPH knockdown alleviates demyelination induced by hypoperfusion

a-d Quantitative analysis mitochondrial load per area (**a**), mitochondrial length (**b**), and mitochondrial diameter (**c**) in Sham+ Scr-shRNA, Sham+ SNPH-shRNA, BCAS+ Scr-shRNA, and BCAS+ SNPH-shRNA mice. Scale bar, 2 µm. For mitochondrial load per area analysis, n=20 visual fields (4 visual fields per mouse, 5 mice per group). For mitochondrial length analysis, n=50 (10 mitochondria per mouse, 5 mice per group). For mitochondrial diameter analysis, n=50 (10 mitochondria per mouse, 5 mice per group). One-way ANOVA $F_{3,24}$ = 5.112, p=0.0071 (**a**); $F_{3,221}$ = 8.269, p<0.001 (**b**); $F_{3,248}$ = 5.316, p=0.0014 (**c**) with Tukey's correction. **d, e, f** Representative TEM images (**d**) and quantitative analysis of G-ratio (**e, f**). For G-ratio analysis, n=80 myelinated axons (20 axons per mouse, 4 mice per group). One-way ANOVA $F_{3,382}$ = 6.967, p=0.0001 with Tukey's correction. Data are represented as means ± SD. (* p<0.05; ** p<0.01; *** p<0.001; ns: non-significant differences).

Fig. S3: In vitro model is established to study hypoperfusion-induced demyelination and mitochondrial accumulation using cultures brain slides

a Representative immunofluorescence images depicting NF (red) and MBP (green) expression in chronic cerebellum slices under normoxic, 12 h LGLO and 48 h LGLO conditions. **b, c, d** Quantitative fluorescence analysis of MBP (**b**), NF (**c**), and NF/MBP (**d**) expression in control, LGLO 12 h, and LGLO 48 h groups. n=8 slices per group. One-way ANOVA $F_{2,18}$ = 45.48, p<0.0001 (**a**); $F_{2,18}$ = 11.2, p=0.0007 (**b**); $F_{2,18}$ = 16.51, p<0.0001 (**c**) with Tukey's correction. **e-h** Representative kymograph (**e**) and quantitative analysis of mitochondrial load per 50 µm (**f**), mitochondrial size (**g**), and percentage of stationary, anterograde, and retrograde mitochondria in axons (**h**) in control, LGLO 12 h, and LGLO 48 h groups. For mitochondrial load per 50 µm analysis, n=20 axons per group. For mitochondrial size analysis, n=400 per group. For percentage of stationary, anterograde, and retrograde mitochondria analysis, n=60 mitochondria per group. One-way ANOVA $F_{2,57}$ = 84.08, p<0.0001 (**f**); $F_{2,1197}$ = 99.82, p<0.0001 (**g**); $F_{2,177}$ =10.36, p<0.0001 for stationary mitochondria; $F_{2,177}$ =12.26, p<0.0001 for anterograde mitochondria; $F_{2,177}$ =6.799, p=0.0014 for retrograde mitochondria (**h**) with Tukey's correction. **i, j** Representative immunoblot (**i**) and quantitative analysis (**j**) of SNPH, Miro1, and Milton expression in cerebellum slices under normoxic, 12 h LGLO, and 48 h LGLO conditions. n=8 slices per group. One-way ANOVA $F_{2,21}$ = 14.22, p=0.0001 for SNPH; $F_{2,21}$ = 1.952, p=0.1669 for Milton; $F_{2,21}$ = 0.959, p=0.3994 for Miro with Tukey's correction. Data are represented as means ± SEM. (* p<0.05; ** p<0.01; *** p<0.001; ns: non-significant differences).

Fig. S4: SNPH knockdown and overexpression efficiency

a, b Representative immunoblot (**a**) and quantitative analysis (**b**) of SNPH expression in cerebellum slices subjected to Scr-shRNA and SNPH-shRNA. n=8 slices per group. Unpaired t-test, t=17.83, df=10, p<0.001. **c, d** Representative immunoblot (**c**) and quantitative analysis (**d**) of SNPH expression in cerebellum slices transfected with empty vector and SNPH overexpression vector (SNPH OE). n=8 slices per group.

Unpaired t-test, t=5.068, df=10, p=0.0005. Data are represented as means ± SEM (* p<0.05; ** p<0.01; *** p<0.001; ns: non-significant differences).

Figures

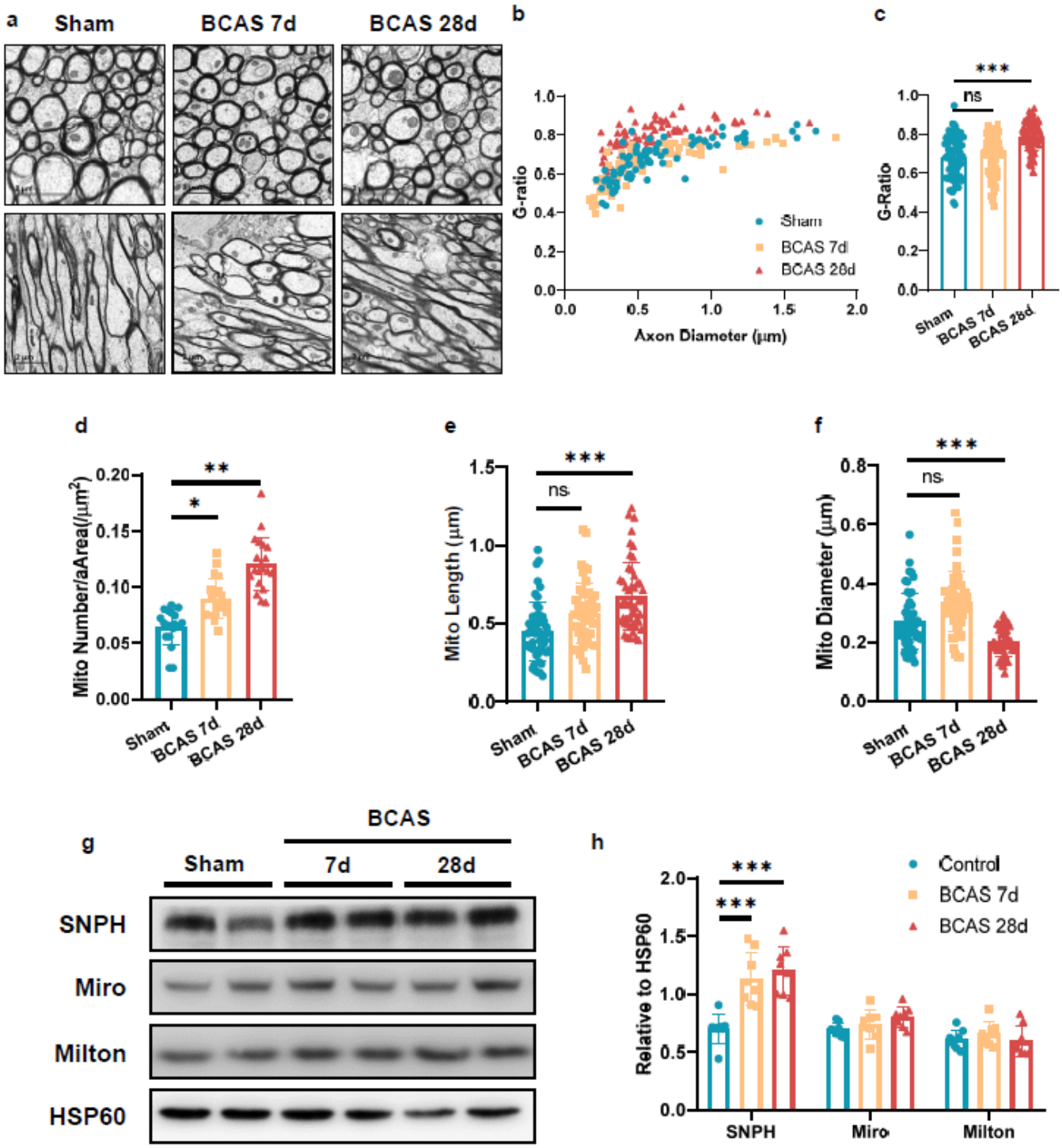

Figure 1

SNPH-mediated mitochondrial accumulation in axons is an early event preceding hy-poperfusion-induced demyelination and cognitive impairment a, b, c Representative TEM images (a) and quantitative analysis of G-ratio (b, c) in Sham-operated, BCAS 7d, and BCAS 28d groups. Scale bar, 2 μm. n=80 myelinated axons (20 axons per mouse, 4 mice per group). One-way ANOVA $F_{2, 237} = 29.96$, $p<0.0001$ with Tukey's correc-tion d, e, f Quantitative TEM analysis of mitochondrial load per area (d), mitochondrial length (e), and mitochondrial diameter (f) in Sham, BCAS 7d, and BCAS 28d groups. Mitochondrial accumulation occurred as early as BCAS day 7 while abnormal mitochondrial length and di-ameter morphology appeared late at BCAS day 28. For mitochondrial load per area analysis, n=20 visual fields (4 visual fields per mouse, 5 mice per group). One-way ANOVA $F_{2, 57} = 42.65$, $p<0.0001$ with Tukey's correction. For mitochondrial length analysis, n=50 (10 mito-chondria per mouse, 5 mice per group). One-way ANOVA $F_{2, 146} = 15.43$, $p<0.0001$ with Tuk-ey's correction. For mitochondrial diameter analysis, n=50 (10 mitochondria per mouse, 5 mice per group). One-way ANOVA $F_{2, 147} = 30.70$, $p<0.0001$ with Tukey's correction. g, h Immunob-lot (g) and quantitative analysis (h) of SNPH, Miro1, and Milton in Sham, BCAS 7d, and BCAS 28d groups. n=8 mice per group. One-way ANOVA $F_{2, 21} = 16.05$, $p<0.0001$ for SNPH; $F_{2, 21} = 2.740$, $p=0.0876$ for Miro1; $F_{2, 21} = 0.6722$, $p=0.5212$ for Milton with Tukey's correction. Data are represented as means ± SD. (* $p<0.05$; ** $p<0.01$; *** $p<0.001$; ns: non-significant differ-ences).

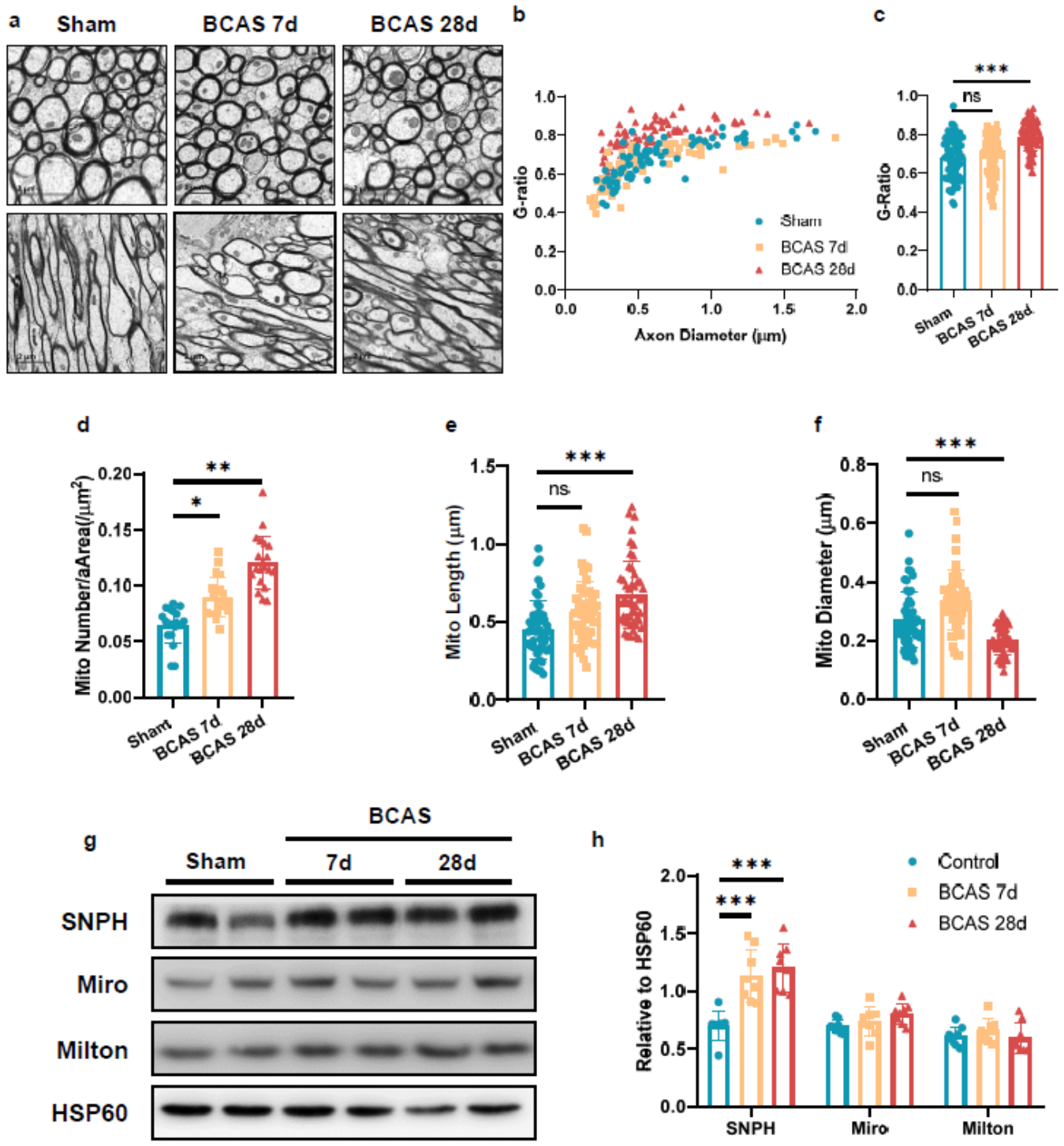

Figure 1

SNPH-mediated mitochondrial accumulation in axons is an early event preceding hy-poperfusion-induced demyelination and cognitive impairment a, b, c Representative TEM images (a) and quantitative analysis of G-ratio (b, c) in Sham-operated, BCAS 7d, and BCAS 28d groups. Scale bar, 2 μm. n=80 myelinated axons (20 axons per mouse, 4 mice per group). One-way ANOVA F2, 237 = 29.96, p<0.0001 with Tukey's correc-tion d, e, f Quantitative TEM analysis of mitochondrial load per area (d), mitochondrial length (e),

and mitochondrial diameter (f) in Sham, BCAS 7d, and BCAS 28d groups. Mitochondrial accumulation occurred as early as BCAS day 7 while abnormal mitochondrial length and di-ameter morphology appeared late at BCAS day 28. For mitochondrial load per area analysis, n=20 visual fields (4 visual fields per mouse, 5 mice per group). One-way ANOVA $F_{2, 57} = 42.65$, $p<0.0001$ with Tukey's correction. For mitochondrial length analysis, n=50 (10 mito-chondria per mouse, 5 mice per group). One-way ANOVA $F_{2, 146} = 15.43$, $p<0.0001$ with Tuk-ey's correction. For mitochondrial diameter analysis, n=50 (10 mitochondria per mouse, 5 mice per group). One-way ANOVA $F_{2, 147} = 30.70$, $p<0.0001$ with Tukey's correction. g, h Immunob-lot (g) and quantitative analysis (h) of SNPH, Miro1, and Milton in Sham, BCAS 7d, and BCAS 28d groups. n=8 mice per group. One-way ANOVA $F_{2, 21} = 16.05$, $p<0.0001$ for SNPH; $F_{2, 21} = 2.740$, $p=0.0876$ for Miro1; $F_{2, 21} = 0.6722$, $p=0.5212$ for Milton with Tukey's correction. Data are represented as means ± SD. (* $p<0.05$; ** $p<0.01$; *** $p<0.001$; ns: non-significant differ-ences).

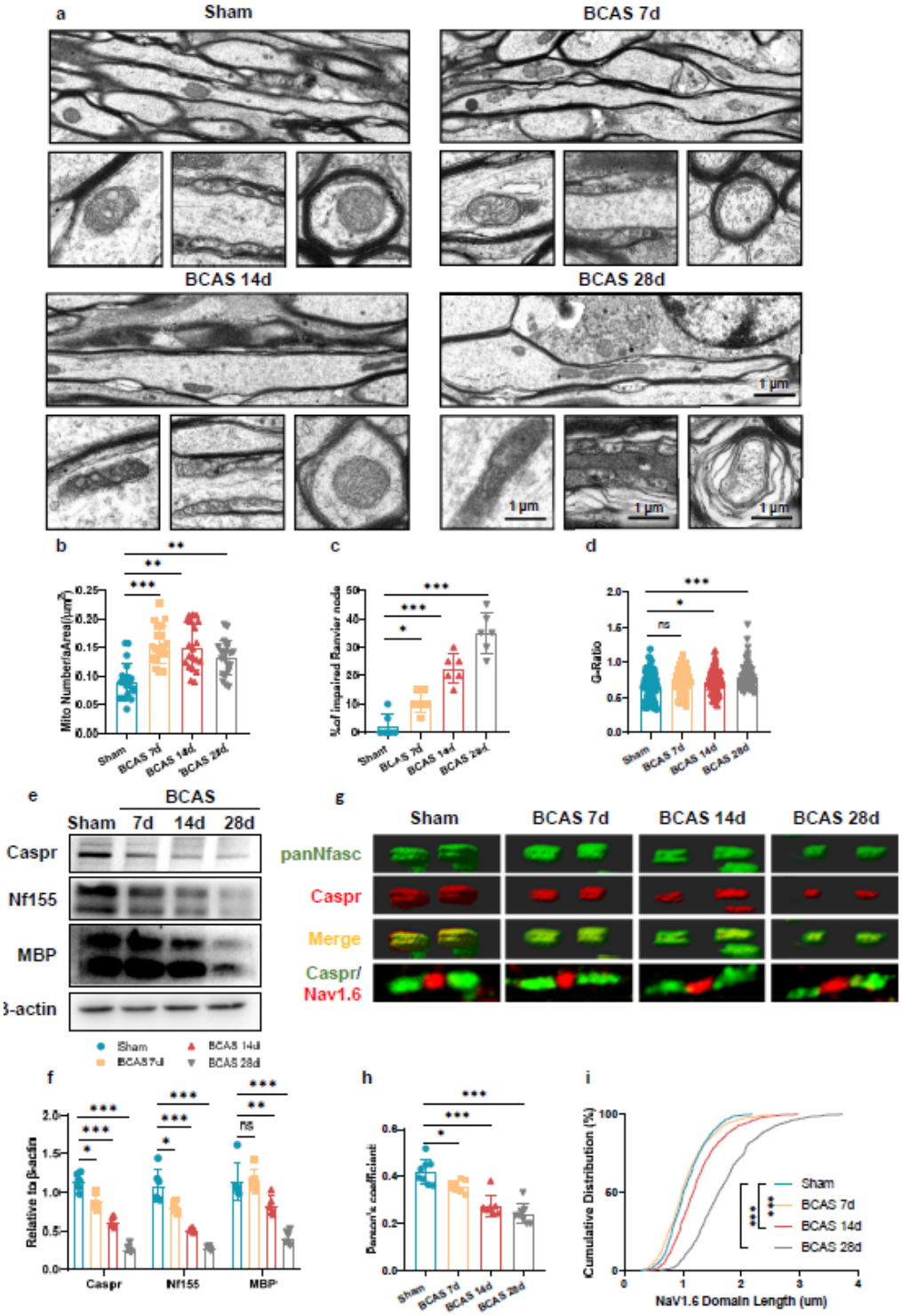

Figure 2

Early mitochondrial accumulation in axons is accompanied by paranode instability a-d Representative TEM images (a) depicting mitochondrial load in axons (top), mitochondrial morphology (bottom left), Ranvier node (bottom middle), myelination status (bottom right) and quantitative analysis of mitochondrial load per area (b), percentage of impaired Ranvier node (c) and G-ratio (d) in Sham, BCAS 7d, BCAS 14 d, and BCAS 28d groups. The early accumula-tion of mitochondria at BCAS day 7 was

accompanied by Ranvier node impairment, whereas myelination status remained normal. Scale bar, 1 μm. For mitochondrial load per area analysis, n=20 visual fields (4 visual fields per mouse, 5 mice per group). For the percentage of Ranvier node impairment analysis, n=6 mice per group. For G-ratio analysis, n=80 myelinated axons (20 axons per mouse, 4 mice per group). One-way ANOVA $F_{3,76} = 14.86$, $p<0.0001$ (b); $F_{3,20} = 44.01$, $p<0.0001$ (c); $F_{3,316} = 6.859$, $p=0.0002$ (d) with Tukey's correction. e, f Immunoblot (e) and quantitative analysis (f) of Caspr, Nf155, and MBP levels in different groups. n=6 mice per group. One-way ANOVA $F_{3, 20} = 153.0$, $p<0.0001$ for Caspr; $F_{3, 20} = 44.04$, $p<0.0001$ for Nf155; $F_{3, 20} = 21.11$, , $p<0.0001$ for MBP with Tukey's correction. g, h, i Representative 3-dimensional confocal images (g) and quantitative analysis of Caspr (red) and panNfasc (green) signal colocalization (h) and the length distribution of Nav1.6 (red) within Caspr (green) (i). For the length distribution of Nav1.6 analysis, n=5 mice per group and 100 Nav 1.6 domains per mouse. For colocalization analysis, n=8 mice per group. One-way ANOVA $F_{3, 28} = 29.04$, $p<0.0001$ with Tukey's correction (h). Data are represented as means ± SD (* $p<0.05$; ** $p<0.01$; *** $p<0.001$; ns: non-significant differences).

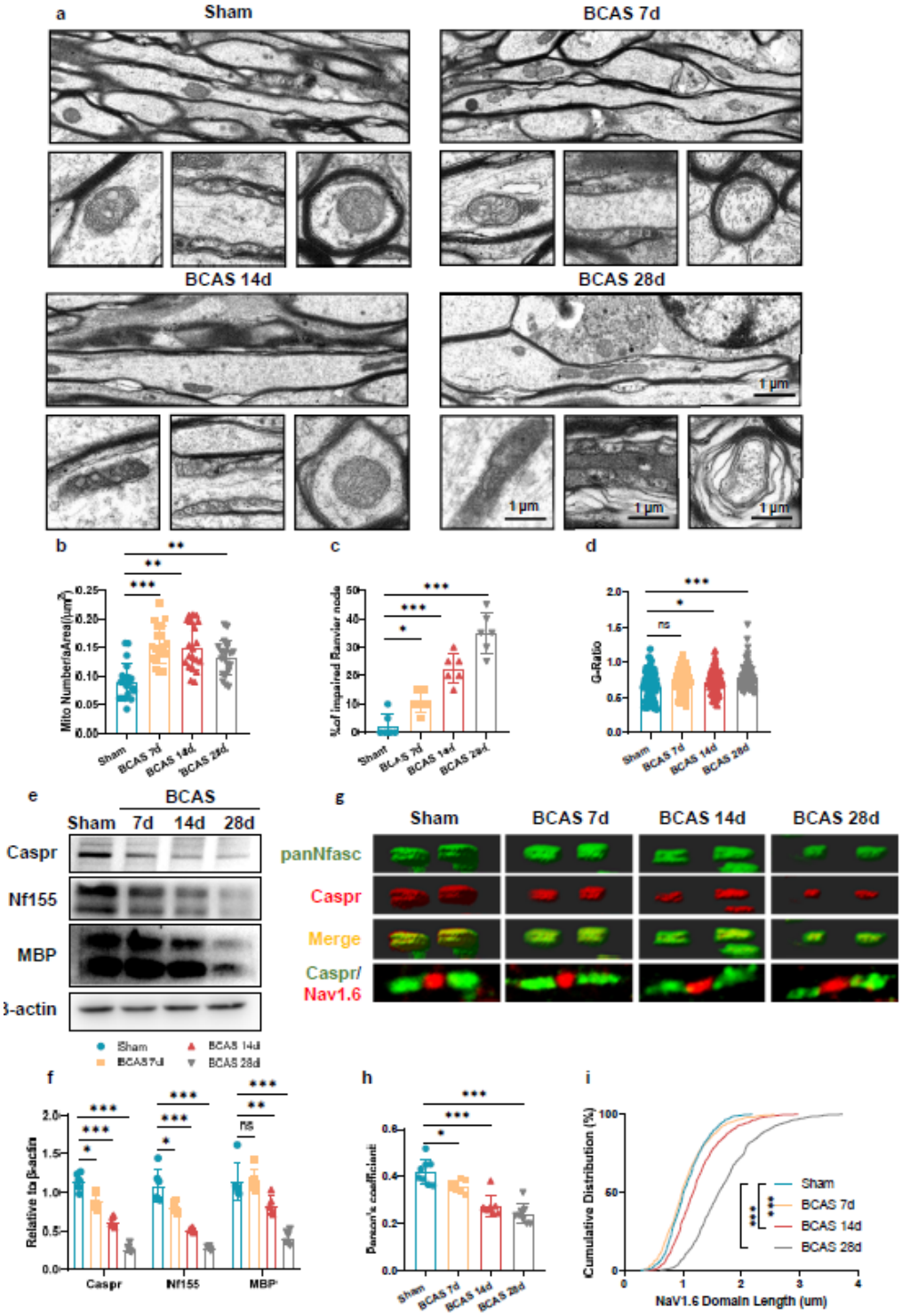

Figure 2

Early mitochondrial accumulation in axons is accompanied by paranode instability a-d Representative TEM images (a) depicting mitochondrial load in axons (top), mitochondrial morphology (bottom left), Ranvier node (bottom middle), myelination status (bottom right) and quantitative analysis of mitochondrial load per area (b), percentage of impaired Ranvier node (c) and G-ratio (d) in Sham, BCAS 7d, BCAS 14 d, and BCAS 28d groups. The early accumula-tion of mitochondria at BCAS day 7 was

accompanied by Ranvier node impairment, whereas myelination status remained normal. Scale bar, 1 μm. For mitochondrial load per area analysis, n=20 visual fields (4 visual fields per mouse, 5 mice per group). For the percentage of Ranvier node impairment analysis, n=6 mice per group. For G-ratio analysis, n=80 myelinated axons (20 axons per mouse, 4 mice per group). One-way ANOVA $F_{3,76} = 14.86$, $p<0.0001$ (b); $F_{3,20} = 44.01$, $p<0.0001$ (c); $F_{3,316} = 6.859$, $p=0.0002$ (d) with Tukey's correction. e, f Immunoblot (e) and quantitative analysis (f) of Caspr, Nf155, and MBP levels in different groups. n=6 mice per group. One-way ANOVA $F_{3, 20} = 153.0$, $p<0.0001$ for Caspr; $F_{3, 20} = 44.04$, $p<0.0001$ for Nf155; $F_{3, 20} = 21.11$, , $p<0.0001$ for MBP with Tukey's correction. g, h, i Representative 3-dimensional confocal images (g) and quantitative analysis of Caspr (red) and panNfasc (green) signal colocalization (h) and the length distribution of Nav1.6 (red) within Caspr (green) (i). For the length distribution of Nav1.6 analysis, n=5 mice per group and 100 Nav 1.6 domains per mouse. For colocalization analysis, n=8 mice per group. One-way ANOVA $F_{3, 28} = 29.04$, $p<0.0001$ with Tukey's correction (h). Data are represented as means ± SD (* $p<0.05$; ** $p<0.01$; *** $p<0.001$; ns: non-significant differences).

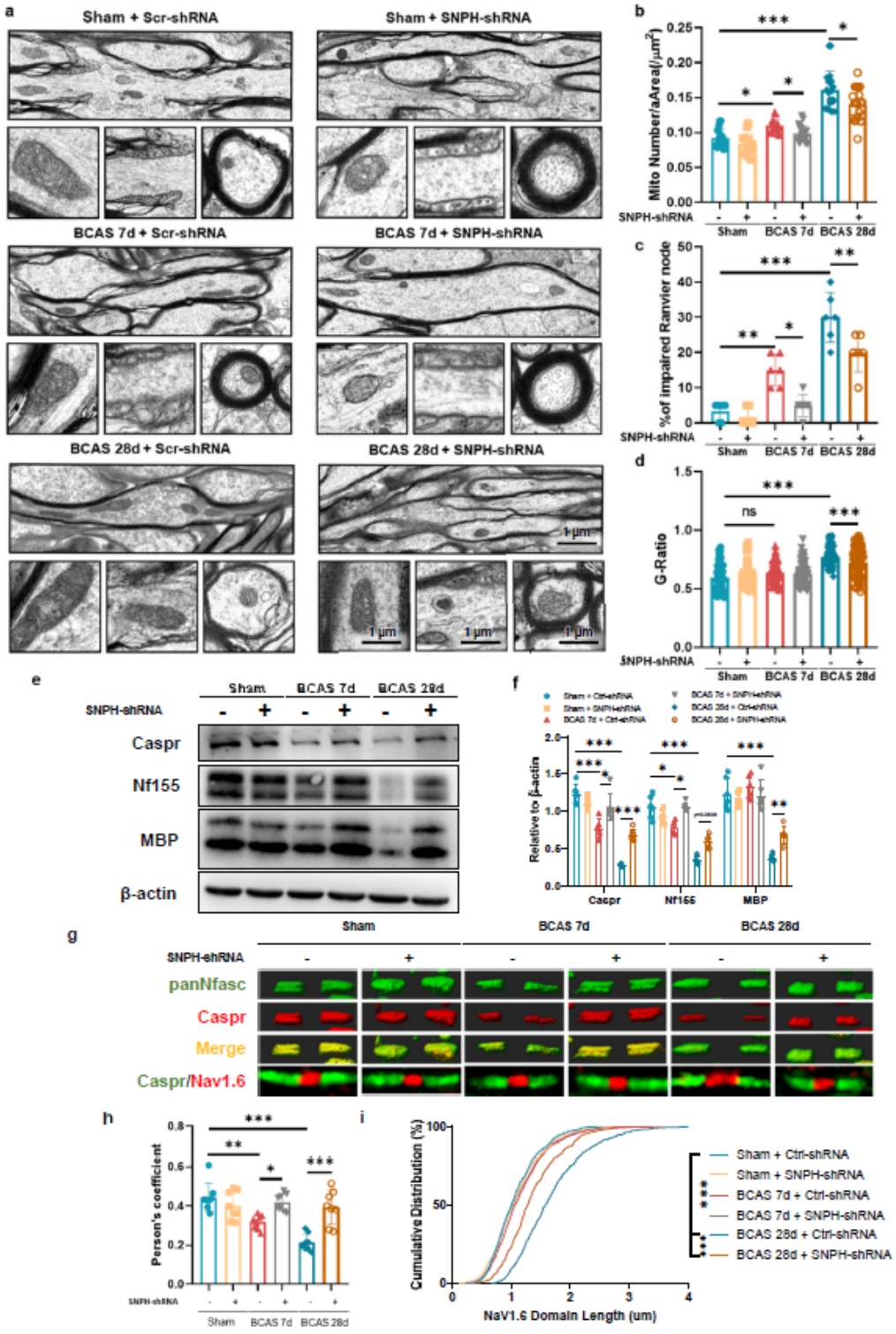

Figure 3

SNPH-mediated mitochondrial accumulation exacerbates demyelination through impairment of paranode stability a-d Representative TEM images depicting mitochondrial load in axons (top), mitochondrial morphology (bottom left), Ranvier node (bottom middle) and myelination status (bottom right), and quantitative analysis of mitochondrial load per area (b), percentage of impaired Ranvier nodes (c) and G-ratio (d) in Sham + Scr-shRNA, Sham + SNPH-shRNA, BCAS 7d + Scr-shRNA, BCAS 7d+ SNPH-shRNA,

BCAS 28d + Scr-shRNA, and BCAS 28d + SNPH-shRNA groups. Scale bar, 1 μm. SNPH knockdown alleviated mitochondrial accumulation in axons and mitigated paranode instability in the early stage (7d) of chronic hypoperfusion and alleviated demyelination on day 28. For mitochondrial load per area analysis, n=20 visual fields (4 visual fields per mouse, 5 mice per group). For the percentage of impaired Ranvier node analysis, n=6 mice per group. For G-ratio analysis, n=80 myelinated axons (20 axons per mouse, 4 mice per group). One-way ANOVA $F_{5,144} = 57.85$, $p<0.0001$ (b); $F_{5,30} = 36.57$, $p<0.0001$ (c); $F_{5,474} = 34.62$, $p<0.0001$ (d) with Tukey's correction. e, f Immunoblot (e) and quantitative analysis (f) of Caspr, NF155, and MBP levels in different groups. n=6 per group. One-way ANOVA $F_{5, 30} = 56.06$, $p<0.0001$ for Caspr; $F_{5, 30} = 54.82$, $p<0.0001$ for Nf155; $F_{5,30} = 39.44$, $p<0.0001$ for MBP with Tukey's correction. g, h, i Representative 3-dimensional confocal images (g) and quantitative analysis of Caspr (red) and panNfasc (green) signal colocalization (h) and the length distribution of Nav1.6 (red) within Caspr (green) (i). For the length distribution of Nav1.6 analysis, n=5 mice per group and 100 Nav 1.6 domains per mouse. For colocalization analysis, n=8 mice per group. One-way ANOVA $F_{5, 42} = 15.19$, $p<0.0001$ with Tukey's correction (h). Data are represented as means ± SD. (* $p<0.05$; ** $p<0.01$; *** $p<0.001$; ns: non-significant differences).

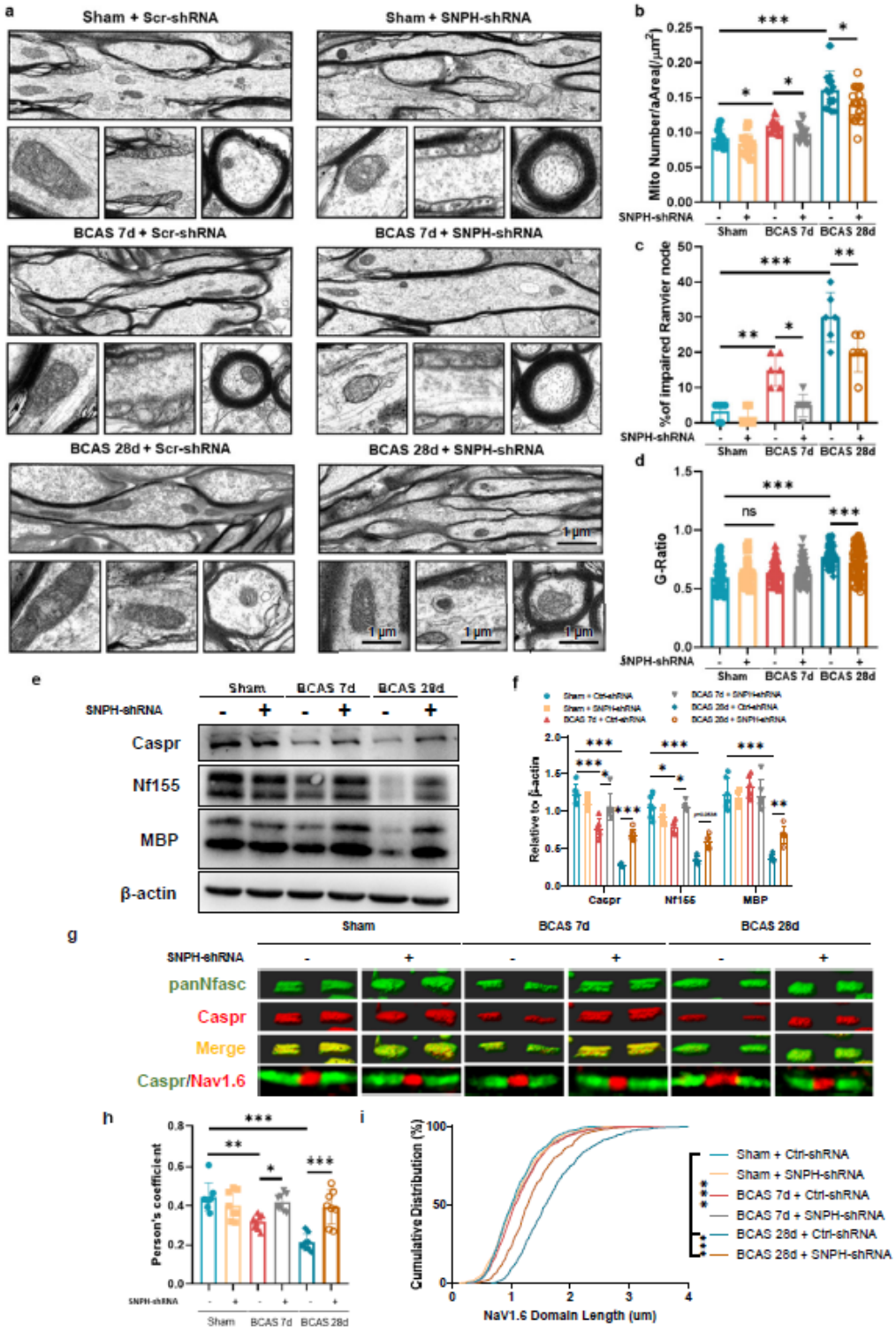

Figure 3

SNPH-mediated mitochondrial accumulation exacerbates demyelination through impairment of paranode stability a-d Representative TEM images depicting mitochondrial load in axons (top), mitochondrial morphology (bottom left), Ranvier node (bottom middle) and myelination status (bottom right), and quantitative analysis of mitochondrial load per area (b), percentage of impaired Ranvier nodes (c) and G-ratio (d) in Sham + Scr-shRNA, Sham + SNPH-shRNA, BCAS 7d + Scr-shRNA, BCAS 7d+ SNPH-shRNA,

BCAS 28d + Scr-shRNA, and BCAS 28d + SNPH-shRNA groups. Scale bar, 1 μm. SNPH knockdown alleviated mitochondrial accumulation in axons and mitigated paranode instability in the early stage (7d) of chronic hypoperfusion and alleviated demyelination on day 28. For mitochondrial load per area analysis, n=20 visual fields (4 visual fields per mouse, 5 mice per group). For the percentage of impaired Ranvier node analysis, n=6 mice per group. For G-ratio analysis, n=80 myelinated axons (20 axons per mouse, 4 mice per group). One-way ANOVA $F_{5,144} = 57.85$, $p<0.0001$ (b); $F_{5,30} = 36.57$, $p<0.0001$ (c); $F_{5,474} = 34.62$, $p<0.0001$ (d) with Tukey's correction. e, f Immunoblot (e) and quantitative analysis (f) of Caspr, NF155, and MBP levels in different groups. n=6 per group. One-way ANOVA $F_{5, 30} = 56.06$, $p<0.0001$ for Caspr; $F_{5, 30} = 54.82$, $p<0.0001$ for Nf155; $F_{5,30} = 39.44$, $p<0.0001$ for MBP with Tukey's correction. g, h, i Representative 3-dimensional confocal images (g) and quantitative analysis of Caspr (red) and panNfasc (green) signal colocalization (h) and the length distribution of Nav1.6 (red) within Caspr (green) (i). For the length distribution of Nav1.6 analysis, n=5 mice per group and 100 Nav 1.6 domains per mouse. For colocalization analysis, n=8 mice per group. One-way ANOVA $F_{5, 42} = 15.19$, $p<0.0001$ with Tukey's correction (h). Data are represented as means ± SD. (* $p<0.05$; ** $p<0.01$; *** $p<0.001$; ns: non-significant differences).

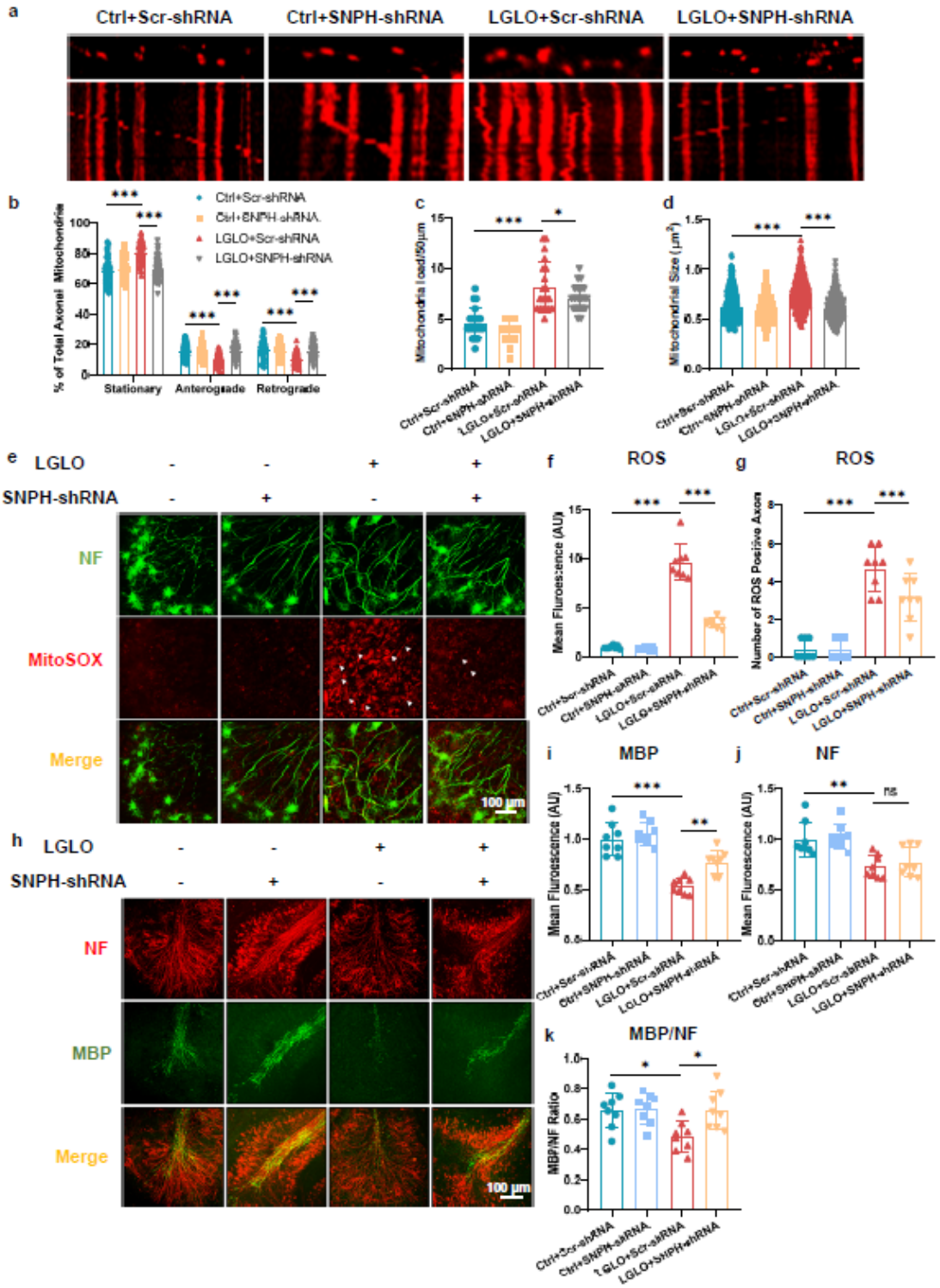

Figure 4

SNPH knockdown alleviates hypoperfusion-induced mitochondrial accumulation and demye-lination by promoting mitochondrial dynamics a-d Representative kymograph (a) and quantitative analysis of the percentage of stationary, an-terograde, and retrograde mitochondria in axons (b), mitochondrial load per 50 μm (c), and mi-tochondrial size (d) in cerebellum slices subjected to Ctrl+ Scr-shRNA, Ctrl+ SNPH-shRNA, LGLO+ Scr-shRNA, and LGLO+ SNPH-shRNA. SNPH knockdown alleviated the LGLO-induced

impairment of retrograde and anterograde mitochondrial transport. For the percentage stationary, anterograde, and retrograde mitochondria analysis, n=60 mitochondria per group. For mitochondrial load per 50 μm analysis, n=20 axons per group. For mitochondrial size anal-ysis, n=400 per group. One-way ANOVA $F_{3,236} = 36.82$, $p<0.0001$ for stationary mitochondria; $F_{3,236} = 23.47$, $p<0.0001$ for anterograde mitochondria; $F_{3,236} = 21.04$, $p<0.0001$ for retrograde mitochondria (b); $F_{3,76} = 29.66$, $p<0.0001$ (c); $F_{3,1596} = 113.6$, $p<0.0001$ (d) with Tukey's correc-tion. e, f, g Representative confocal images (e) and quantitative analysis of ROS expression (f) and the number of ROS positive axons (g). Scale bar, 100 μm. SNPH knockdown mitigated LGLO-induced ROS generation. n=8 slices per group. One-way ANOVA $F_{3, 28} = 152.3$, $p<0.0001$ (f); $F_{3, 28} = 40.76$, $p<0.0001$ with Tukey's correction. h-k Representative confocal im-ages (h) and quantitative analysis of MBP (green) expression (i), NF (red) expression (j), and the MBP/NF ratio (k). SNPH knockdown alleviated LGLO-induced demyelination. Scale bar, 100 μm. n=8 slices per group. One-way ANOVA $F_{3,28} = 30.03$, $p<0.0001$ (i); $F_{3,28} = 9.266$, $p=0.0002$ (j); $F_{3,28} = 5.148$, $p=0.0058$ (k) with Tukey's correction. Data are represented as means ± SEM. (* $p<0.05$; ** $p<0.01$; *** $p<0.001$; ns: non-significant differences).

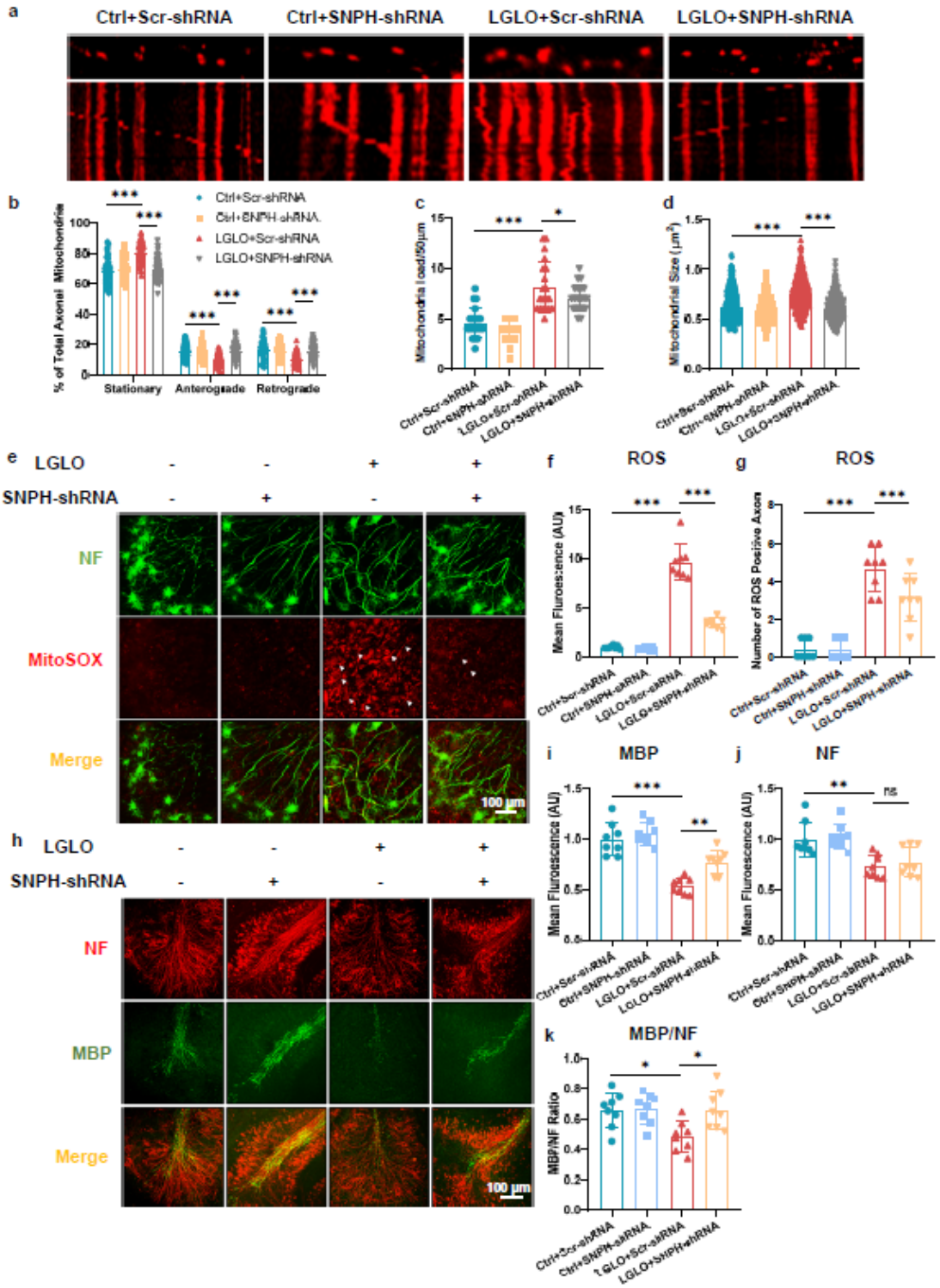

Figure 4

SNPH knockdown alleviates hypoperfusion-induced mitochondrial accumulation and demye-lination by promoting mitochondrial dynamics a-d Representative kymograph (a) and quantitative analysis of the percentage of stationary, an-terograde, and retrograde mitochondria in axons (b), mitochondrial load per 50 μm (c), and mi-tochondrial size (d) in cerebellum slices subjected to Ctrl+ Scr-shRNA, Ctrl+ SNPH-shRNA, LGLO+ Scr-shRNA, and LGLO+ SNPH-shRNA. SNPH knockdown alleviated the LGLO-induced

impairment of retrograde and anterograde mitochondrial transport. For the percentage stationary, anterograde, and retrograde mitochondria analysis, n=60 mitochondria per group. For mitochondrial load per 50 μm analysis, n=20 axons per group. For mitochondrial size anal-ysis, n=400 per group. One-way ANOVA $F_{3,236} = 36.82$, $p<0.0001$ for stationary mitochondria; $F_{3,236} = 23.47$, $p<0.0001$ for anterograde mitochondria; $F_{3,236} = 21.04$, $p<0.0001$ for retrograde mitochondria (b); $F_{3,76} = 29.66$, $p<0.0001$ (c); $F_{3,1596} = 113.6$, $p<0.0001$ (d) with Tukey's correc-tion. e, f, g Representative confocal images (e) and quantitative analysis of ROS expression (f) and the number of ROS positive axons (g). Scale bar, 100 μm. SNPH knockdown mitigated LGLO-induced ROS generation. n=8 slices per group. One-way ANOVA $F_{3, 28} = 152.3$, $p<0.0001$ (f); $F_{3, 28} = 40.76$, $p<0.0001$ with Tukey's correction. h-k Representative confocal im-ages (h) and quantitative analysis of MBP (green) expression (i), NF (red) expression (j), and the MBP/NF ratio (k). SNPH knockdown alleviated LGLO-induced demyelination. Scale bar, 100 μm. n=8 slices per group. One-way ANOVA $F_{3,28} = 30.03$, $p<0.0001$ (i); $F_{3,28} = 9.266$, $p=0.0002$ (j); $F_{3,28} = 5.148$, $p=0.0058$ (k) with Tukey's correction. Data are represented as means ± SEM. (* $p<0.05$; ** $p<0.01$; *** $p<0.001$; ns: non-significant differences).

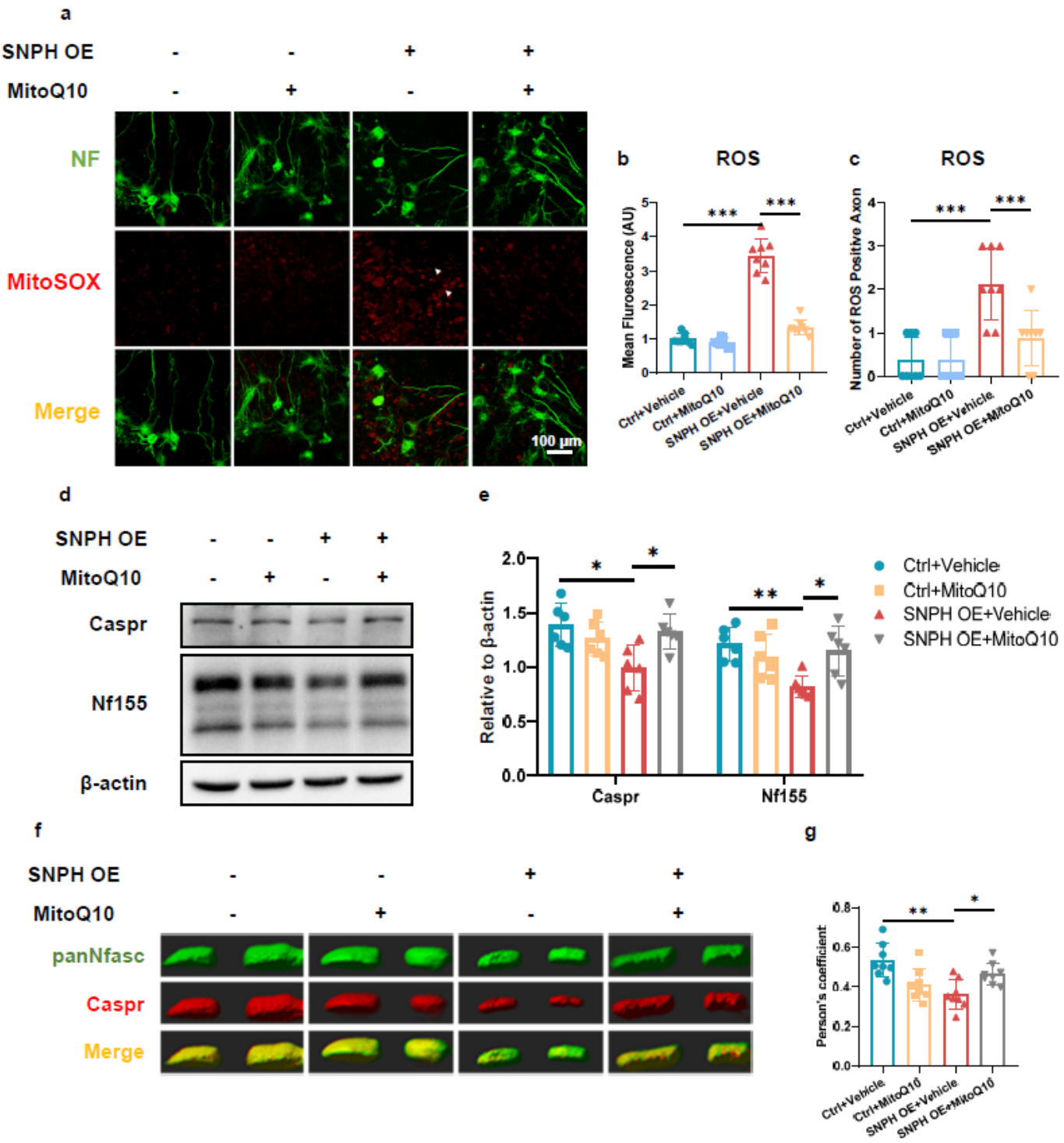

Figure 5

Accumulated mitochondria in axons damage paranode structure through ROS production a, b, c Representative confocal images (a) and quantitative analysis of ROS production (b) and the number of ROS positive axons (c) in different treated cerebellum slices. SNPH overexpres-sion elevated ROS production in normoxic conditions. Scale bar, 100 μm. n=8 slices per group. One-way ANOVA $F_{3,28} = 130.6$, $p<0.0001$(b); $F_{3,28} = 13.29$, $p<0.0001$ (c) with Tukey's correc-tion. d, e Immunoblot (d) and

quantitative analysis of Caspr and NF155 levels (e) in different groups. n=6 slices per group. One-way ANOVA $F_{3,20} = 5.481$, $p=0.0065$ for Caspr; $F_{3,20} = 5.594$, $p<0.0001$ for NF155 with Tukey's correction. f, g, h Representative 3-dimensional con-focal images (f) and quantitative analysis of the colocalization of Caspr (red) and panNfasc (green) signals (g) and the length distribution of Nav1.6 (red) within Caspr (green) (h). For the length distribution of Nav1.6 analysis, n=5 slices per group and 100 Nav 1.6 domains per slice. For colocalization analysis, n=8 slices per group. One-way ANOVA $F_{3,28} = 7.808$, $p=0.0006$ with Tukey's correction. Data are represented as means ± SEM. (* $p<0.05$; ** $p<0.01$; *** $p<0.001$; ns: non-significant differences).

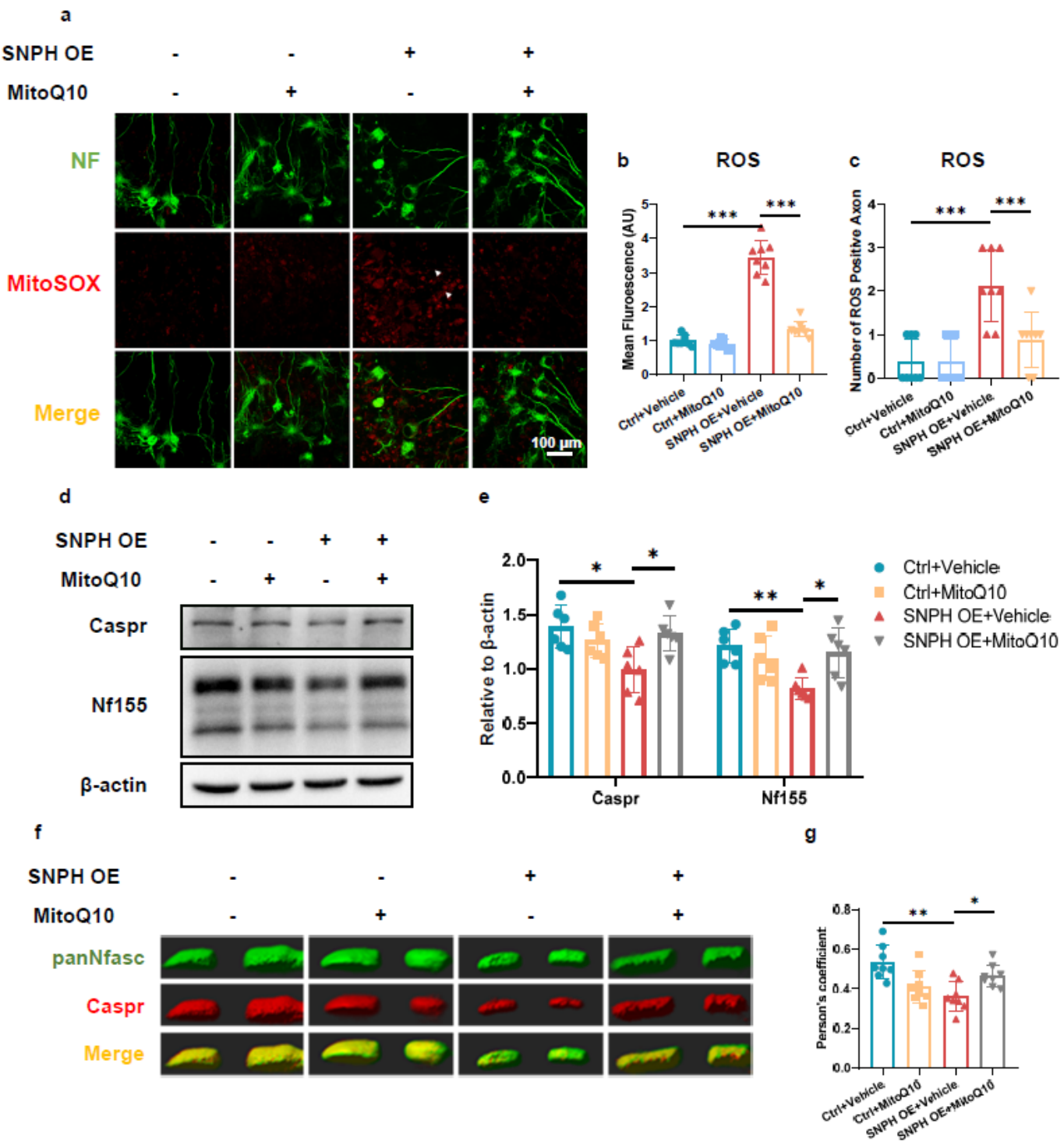

Figure 5

Accumulated mitochondria in axons damage paranode structure through ROS production a, b, c Representative confocal images (a) and quantitative analysis of ROS production (b) and the number of ROS positive axons (c) in different treated cerebellum slices. SNPH overexpres-sion elevated ROS production in normoxic conditions. Scale bar, 100 μm. n=8 slices per group. One-way ANOVA $F_{3,28} = 130.6$, $p<0.0001$(b); $F_{3,28} = 13.29$, $p<0.0001$ (c) with Tukey's correc-tion. d, e Immunoblot (d) and

quantitative analysis of Caspr and NF155 levels (e) in different groups. n=6 slices per group. One-way ANOVA $F_{3,20} = 5.481$, $p=0.0065$ for Caspr; $F_{3,20} = 5.594$, $p<0.0001$ for NF155 with Tukey's correction. f, g, h Representative 3-dimensional con-focal images (f) and quantitative analysis of the colocalization of Caspr (red) and panNfasc (green) signals (g) and the length distribution of Nav1.6 (red) within Caspr (green) (h). For the length distribution of Nav1.6 analysis, n=5 slices per group and 100 Nav 1.6 domains per slice. For colocalization analysis, n=8 slices per group. One-way ANOVA $F_{3,28} = 7.808$, $p=0.0006$ with Tukey's correction. Data are represented as means ± SEM. (* $p<0.05$; ** $p<0.01$; *** $p<0.001$; ns: non-significant differences).

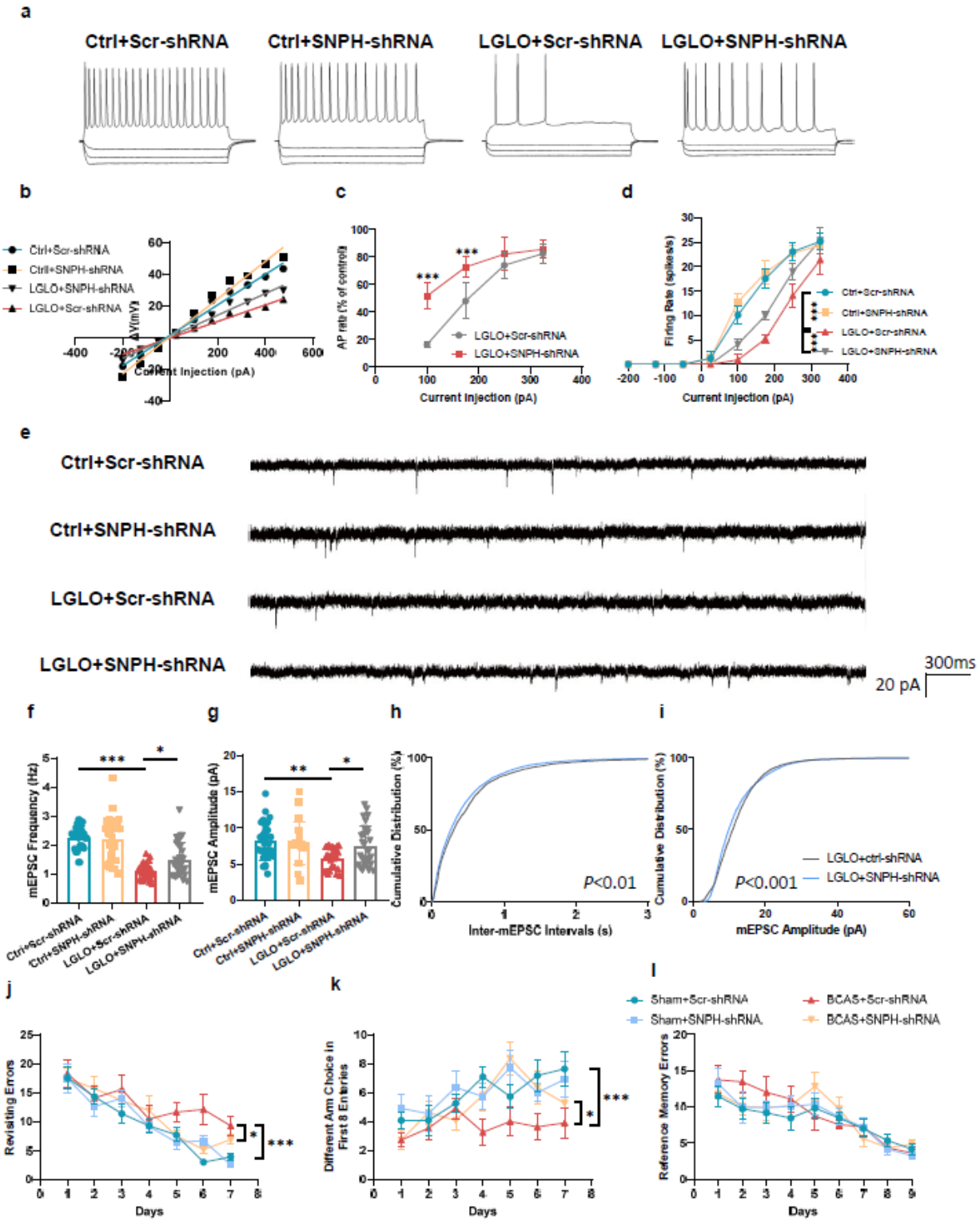

Figure 6

SNPH knockdown enhances mitochondrial dynamics and promotes synaptic activity a-d Representative firing responses (a) to depolarizing (175 pA) and hyperpolarizing (-50, -135, and -200 pA) current injections and quantitative analysis of input resistance (b), percentage of control firing rates (c), and firing rate responses to a series of linear current injections (-200 to -50 pA) (d) in different treated cerebellum slices. For the percentage of control firing rates analy-sis, n=9 neurons per group (3 neurons per slices).

For firing rate responses to a series of linear current injection analysis, n=9 neurons per group (3 neurons per slices). Two-way ANOVA for interaction factor $F_{3,64} = 12.14$, $p<0.0001$ (c); $F_{21,224} = 38.93$, $p<0.0001$ (d) with Dunnett's post-hoc test. e-i Representative mEPSC traces (e) and quantitative analysis of mEPSC frequency (f), amplitude (g), and cumulative distribution of inter-mEPSC interval (h) and mEPSC amplitude (i). Under LGLO conditions, intrinsic neuronal excitability and synapse function showed remarkable improvement after SNPH knockdown. For mEPSC frequency, n=30 per group. For mEPSC amplitude, n=30 per group. For cumulative distribution of inter-mEPSC interval, n=4291 per group. For cumulative distribution of mEPSC amplitude, n=4319 per group. One-way ANOVA $F_{3,116} = 33.74$, $p<0.0001$ (f); $F_{3,116} = 5.431$, $p=0.0016$ (g) with Tukey's correction. j, k, l Working and reference memory were assessed using the 8-arm maze test. Impaired work-ing memory in BCAS mice was rescued by down-regulating of SNPH, as evidenced by less re-visiting errors (j) and more different choices (k) in BCAS+ SNPH-shRNA group. No significant difference in spatial reference memory was observed between different groups (l). n=11 mice in each group. Two-way ANOVA for interaction factor $F_{18,240} = 12.12$, $p<0.0001$ (j); $F_{18,240} = 11.99$, $p<0.0001$ (k); $F_{24,320} = 7.787$, $p<0.0001$ (l) with Dunnett's post-hoc test. Data are repre-sented as means ± SD. (* $p<0.05$; ** $p<0.01$; *** $p<0.001$; ns: non-significant differences).

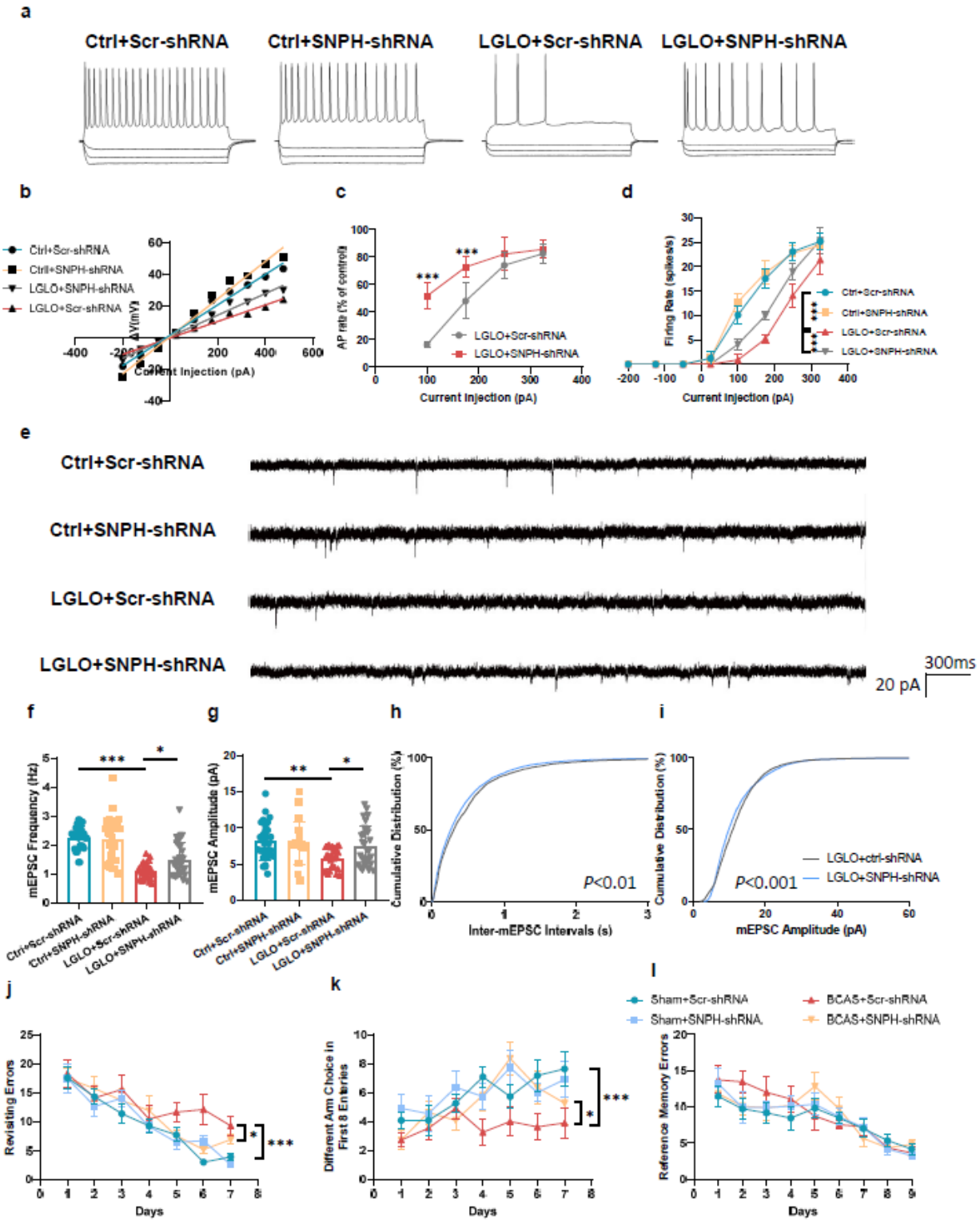

Figure 6

SNPH knockdown enhances mitochondrial dynamics and promotes synaptic activity a-d Representative firing responses (a) to depolarizing (175 pA) and hyperpolarizing (-50, -135, and -200 pA) current injections and quantitative analysis of input resistance (b), percentage of control firing rates (c), and firing rate responses to a series of linear current injections (-200 to -50 pA) (d) in different treated cerebellum slices. For the percentage of control firing rates analy-sis, n=9 neurons per group (3 neurons per slices).

For firing rate responses to a series of linear current injection analysis, n=9 neurons per group (3 neurons per slices). Two-way ANOVA for interaction factor $F_{3,64} = 12.14$, $p<0.0001$ (c); $F_{21,224} = 38.93$, $p<0.0001$ (d) with Dunnett's post-hoc test. e-i Representative mEPSC traces (e) and quantitative analysis of mEPSC frequency (f), amplitude (g), and cumulative distribution of inter-mEPSC interval (h) and mEPSC amplitude (i). Under LGLO conditions, intrinsic neuronal excitability and synapse function showed re-markable improvement after SNPH knockdown. For mEPSC frequency, n=30 per group. For mEPSC amplitude, n=30 per group. For cumulative distribution of inter-mEPSC interval, n=4291 per group. For cumulative distribution of mEPSC amplitude, n=4319 per group. One-way ANOVA $F_{3,116} = 33.74$, $p<0.0001$ (f); $F_{3,116} = 5.431$, $p=0.0016$ (g) with Tukey's correction. j, k, l Working and reference memory were assessed using the 8-arm maze test. Impaired work-ing memory in BCAS mice was rescued by down-regulating of SNPH, as evidenced by less re-visiting errors (j) and more different choices (k) in BCAS+ SNPH-shRNA group. No significant difference in spatial reference memory was observed between different groups (l). n=11 mice in each group. Two-way ANOVA for interaction factor $F_{18,240} = 12.12$, $p<0.0001$ (j); $F_{18,240} = 11.99$, $p<0.0001$ (k); $F_{24,320} = 7.787$, $p<0.0001$ (l) with Dunnett's post-hoc test. Data are repre-sented as means ± SD. (* $p<0.05$; ** $p<0.01$; *** $p<0.001$; ns: non-significant differences).

Supplementary Files

This is a list of supplementary files associated with this preprint. Click to download.

- SulplementaryData.pdf
- SulplementaryData.pdf
- soursedata.xlsx
- soursedata.xlsx